INVESTIGATION OF PARTIALLY COHERENT INTERACTION IN FIBER BRAGG GRATING STABILIZED 980-NM PUMP MODULES

INVESTIGATION OF PARTIALLY COHERENT INTERACTION IN FIBER BRAGG GRATING STABILIZED 980-NM PUMP MODULES

By
JINGCONG WANG, B.Sc, M.Sc

A Thesis
Submitted to the School of Graduate Studies
in Partial Fulfillment of the Requirements
for the Degree
Master of Applied Science

McMaster University

MASTER OF APPLIED SCIENCE MCMASTER UNIVERSITY

(Engineering Physics) Hamilton, Ontario

TITLE: Investigation of Partially Coherent Interaction in Fiber Bragg Grating Stabilized 980-nm Pump Modules

AUTHOR: Jingcong Wang, B. Sc. (Northeast Normal University of China)
M. Sc. (University of Science and Technology of China)

SUPERVISOR: Professor D. T. Cassidy

NUMBER OF PAGES: x, 80

ABSTRACT

Partially coherent interaction of the feedback light with the field in the laser cavity is affirmed with the fiber Bragg grating (FBG) stabilized 980-nm pump lasers, on the contrast of normally accepted totally incoherent state of operation in the "coherence collapse" regime. Coherence parameter γ was defined in this paper to identify the fraction of feedback light working coherently. It is shown that γ can be determined by fitting the measured power-difference versus pumping-rate curve to the simulation results. Experiments confirm that coherence parameter γ decreases while the distance between the FBG and the laser facet increases, and *vice versa*. While, if the device is kept operating in the "coherence-collapse" regime, γ would not change with the amount of feedback. This work will be help to improve the performance of the high power FBG stabilized 980-nm pump laser.

ACKNOWLEDGEMENTS

I would like to express my gratitude to my supervisor, Dr. D.T.Cassidy, for his guidance and support throughout the course of this work.

I would like to thank Dr. Douglas Bruce and my friend Jian Yang for all the suggestions and apparatus supply in my experimental measurements.

I would also like to thank my labmates Jay Welbourn, Gord Morrison, Huiling Wang, Sean Woodworth, Aaron Vandermeer, Sam KarKin Lam, and Mark Fritz, for the valuable discussions and the pleasures we have had together.

My husband and my son deserve the most thanks of all. Without their love and support, I would not have been able to finish this work in time.

TABLE OF CONTENTS

LIST OF FIGURES

LIST OF TABLES

CHAPTER 1 INTRODUCTION

1.1 Semiconductor laser

Lasers are devices that generate and amplify coherent radiation at frequencies in the infrared, visible or ultraviolet region of the electromagnetic spectrum. Lasers emit light in a very narrow wavelength band, and this spectral purity is one of the most important properties of the devices. Although lasers come in a great variety of forms and may emit light at widely different wavelengths, they all consist of the same essential elements. These elements are: (1) a gain medium, through which the electromagnetic radiation can be amplified; (2) a pumping process to excite atoms or molecules of the gain medium into higher energy levels; and, (3) a set of partial feedback elements that allow a beam of radiation to either bounce back into the gain medium or to exit the laser as output. A semiconductor diode laser is a laser whose gain medium is made of direct band gap semiconductor materials.

A semiconductor laser consists of a single crystal of direct band gap semiconductor material. To date, most laser diodes have been made using GaAs, $Ga_{1-x}Al_xAs$ or $In_{1-x}Ga_xAs_{1-y}P_y$, but other materials will no doubt eventually be used to obtain emission at different wavelengths. The most basic structure of the laser diode is a p-n junction [1]. When this p-n junction is forward biased, the holes in the p-type region are injected into the n-type region, while electrons in the n-type region are injected into the p-type region. When an electron meets a hole, they combine emitting a photon of energy nearly equal to the band gap energy. The region where these activities occur is called the active region.

The wavelength of emission of a diode laser depends mainly on the type of semiconductor material that it is made of. However, this lasing wavelength can vary slightly with operating temperature and current of the laser. Furthermore, if the p-n junction is made from a quaternary crystal, the diode laser has an emission wavelength which is set by varying the fraction x and y.

Ohmic contacts are made to both p- and n-regions to permit the flow of electrical current, which is the energy required to produce the inverted population in the active region. The directivity of the output from the semiconductor is not sharp. The output spreads out by as much as 30 degrees. This is because the light is emitted from the active region, a very small area whose sizes are less than 2-3 μm. The intensity of the emitted light is a function of injection current and it is found that this intensity increases rapidly above a certain current I_{th}, while below I_{th} it is rather weak. I_{th} is the starting current for laser oscillation and is called the threshold current. The partially reflecting end faces of the laser diode, formed by cleaving the laser chip along a crystal plane, provide an optical feedback that leads to the establishment of one or more longitudinal modes. Longitudinal modes of the laser are centered at frequencies where a half-integral number of wavelengths equal the length of the optical cavity. Thus, $m\lambda/2 = nL$, where L is the length of the laser, n is the index of refraction of the laser material, and λ is the wavelength of emitted light. The separation in frequency of these longitudinal modes are given by the free spectral range (FSR) of laser cavity, $FSR = c/2n_gL$ where n_g is the group index of refraction. Normally, a laser will oscillate on a number of modes. To achieve single longitudinal mode operation, additional arrangement must be made to suppress all but the preferred mode of the laser. Such specialized devices include DFB, DBR laser, and short external cavity laser. DFB and DBR lasers are out of vision of this research. We will talk about diode lasers with external cavity in this thesis.

1.2 Diode lasers with external cavity

The effects of reflection which feed light back into semiconductor lasers have been studied extensively. It is often beneficial to operate laser diodes with optical feedback, as provided, for example, by an external mirror according to Fig. 1.1.

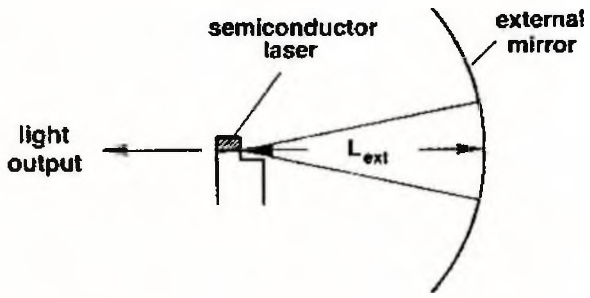

Fig. 1.1 Semiconductor laser in external feedback configuration

This external mirror may serve for the selection of a distinct longitudinal mode of the Fabry-Perot laser in order to get better side-mode suppression [2]. If the longitudinal mode selection is provided by a grating reflector, the external feedback may be used for tuning the wavelength [3] [4] or for a considerable linewidth narrowing [5]. An external cavity may also be useful for reducing the laser chirp [6]. With the process of integrated optics, laser diodes together with external cavities may be also integrated [7], yielding a potential for economic production of external cavity devices.

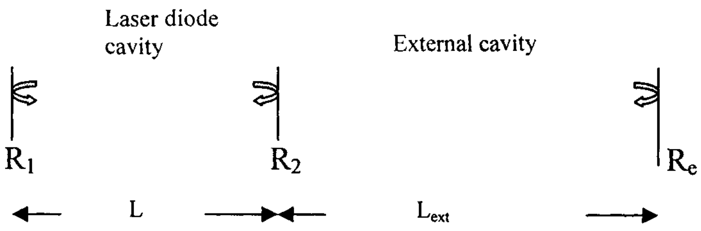

Fig.1.2 Schematic arrangement of a laser diode cavity with external optical feedback

Due to the presence of an external cavity, the phase condition which chooses the longitudinal modes and the loss condition which defines the threshold of the modes have to be modified to the laser, so will the lasing frequency and the threshold gain.

Assuming the polarization of the reflected light is identical to the polarization of the emitted light, the required gain in an external cavity laser for threshold is changed [8] to:

$$g_c = g_{th} - |C_e| \frac{2\eta\sqrt{R_e}}{L} \cos(\phi_{ext}) \tag{1.1}$$

with the phase of the reflected light $\phi_{ext} = 2\pi\nu\tau_{ext}$, where ν is the optical frequency and τ_{ext} is the external roundtrip time delay. g_{th} denotes the threshold gain without external feedback. $|C_e|$ is the coupling coefficient from the laser to the external cavity ($C_e = (1-\sqrt{R_1 R_2})/2\sqrt{R_1}$) for Fabry-Perot lasers with facet reflectivity as shown in Fig. 1.2. η is the coupling efficiency from the laser to the external cavity. Depending on the phase ϕ_{ext} of the external reflected light the required gain for threshold is either reduced or increased. The maximum threshold gain reduction occurs if ϕ_{ext} is an integer multiple of 2π.

Possible modes of the laser with feedback are characterized by the threshold gain and the phase condition, requiring an effective round trip phase change of $\Delta\phi_L = 0$ (or multiples of 2π). For deriving this round trip phase, a change in threshold gain yielding a change in the refractive index through the linewidth enhancement factor α has to be taken into account, yielding finally [9]:

$$\Delta\phi_L = \frac{\tau_L}{\tau_{ext}}(2\pi\tau_{ext}(\nu-\nu_{th}) + C\sin(2\pi\nu\tau_{ext} + \arctan\alpha)) \qquad (1.2)$$

with τ_L – the round trip time of the solitary laser and ν_{th} – the lasing frequency without external optical feedback. C denotes the feedback parameter:

$$C = \eta\sqrt{R_e}\frac{2|C_e|\tau_{ext}}{\tau_L}\sqrt{1+\alpha^2} \qquad (1.3)$$

For $C < 1$, the round trip phase change $\Delta\phi_L$ is monotonic with respect to the optical frequency as for the solid curve in Fig. 1.3 yielding a single zero for $\Delta\phi_L$. Whereas for $C > 1$, the $\Delta\phi_L$ versus ν-characteristics may have several zeros, so that eventually several cavity modes around ν_{th} may start lasing.

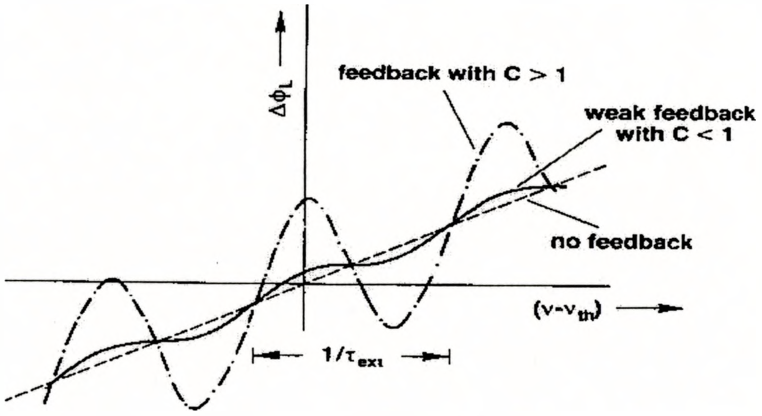

Fig.1.3 The round trip phase change $\Delta\phi_L$ versus optical frequency ν with and without optical feedback. The phase condition for the compound cavity is satisfied for $\Delta\phi_L = 0$

In conclusion, the feedback sensitivity of laser diodes is governed essentially by the feedback parameter C. For a given laser, (facet reflectivity R and round trip delay τ_L), low external cavity reflectivity R_e and a small round trip delay τ_{ext} are required for getting low C. That is the reason why tunable lasers are achieved through short external cavity [3].

Due to optical feedback, the spectral width may be influenced considerably. Many researches have been done over the past two decades on this topic [5] [10-13]. Under weak or moderate levels of feedback,

$$\Delta\nu = \frac{\Delta\nu_0}{[1 + C\cos(\phi_{ext} + \arctan\alpha)]^2} \tag{1.3}$$

where $\Delta\nu_0$ is the linewidth of the solitary laser without feedback. According to K. Petermann [8], the linewidth depends on the feedback phase ϕ_{ext}, and $\Delta\nu_{min} = \Delta\nu_0/(1+C)^2$, $\Delta\nu_{max} = \Delta\nu_0/(1-C)^2$. Even the very low feedback with $C \approx 1$ may yield a very large linewidth broadening. This linewidth broadening is actually the splitting from a single external cavity mode to a dual mode, which should not be confused with the coherence collapse under high feedback being discussed later.

The relationship between linewidth and amount of feedback has been studied sufficiently by R.W.Tkach and A.R.Chraplyvy [14]. Five regimes have been identified according to the feedback power ratio which is defined as $f_{ext} = \eta^2 R_e$. The five regimes of feedback effects are:

I. At the lowest levels of feedback, narrowing or broadening of the emission line is observed, depending on the phase of the feedback. The power ratio of feedback in this regime is under -70 dB($C < 1$).

II. When the feedback level lies between ~ -70 dB and ~ -45 dB, the broadening, which is observed at regime I for out of phase feedback, changes to a splitting of emission line with rapid mode hopping.

III. As the feedback is increased further, the mode hopping is suppressed and the laser is observed to operate on a single narrow line. This level of feedback effect does not depend on the distance to the reflection. This regime occupies only a very small range of feedback, from ~ -45 dB to ~ -39 dB.

IV. With higher feedback levels, line broadening by several orders of magnitude is observed, this phenomenon is known as "coherence collapse" [15] [16] because of the drastic reduction in the coherence length of the laser. The feedback level of this regime is -40 dB~ -10 dB. This regime is usually not desirable for a tunable laser realized by short external cavity. But it is the regime this thesis will work on.

V. When the feedback levels are higher than -10 dB, stable single mode oscillation with a very narrow linewidth occurs again. This level of feedback is obtained only when the facet through which light is fed back into the laser cavity is highly AR coated. In this regime, the laser ideally operates in a long cavity with a short active region and the feedback dominates the field in the diode laser. The linewidth in this configuration is narrowed for all phases of returned light, and is generally insensitive to all other reflections.

During the past years, extensive work has been done on the linewidth enhancement factor utilizing short external cavity (SXC) diode lasers [17]. It is found that the linewidth enhancement factor strongly depends on the emission wavelength, and is fairly independent of the output powers for SXC diode lasers. Bonnell and Cassidy [18] have found that the fraction of light reflected back to the diode laser is less than 5×10^{-4} for a short external cavity. In this case, the feedback parameter C is less than 0.1 which lies in regime I. Coherence collapse of regime IV is what researchers try to avoid in the short-external cavity tunable laser. On the other extreme, regime V is an attractive domain to work within tunable laser, but this will require wide bandwidth AR coating for diode laser in the front facet [19].

Although "coherence collapse" is not applicable in tunable lasers, it works in the field of power and temperature stabilization of diode lasers. Fiber Bragg grating (FBG) stabilized semiconductor lasers take advantage of coherence collapse feedback to obtain high kink output power, high temperature operation. 980-nm pump laser for EDFA, which is the research topic of this thesis, is one of such successful examples.

1.3 980-nm pump laser with fiber Bragg grating(FBG) feedback

980-nm laser diodes are essential components for optical amplifying systems, which fulfill the increasing requirements of rapid and large capacity communications. 980-nm LDs are the most promising devices to provide excitation light sources for erbium-doped fiber amplifiers (EDFAs). Compared with the other main wavelength option for pumping such as 1480-nm, the advantages of employing 980-nm are lower noise figure [20] and lower power-consumption. However, one of the difficulties of using 980-nm pumping is the narrower absorption range of an erbium doped fiber compared with 1480-nm pumps. It is essential to achieve wavelength stabilization and control over an extended operating range and a large variety of pump lasers. The passive locking of 980-nm pump to external cavity fiber Bragg grating has been considered and successfully employed [21], [22]. Thus, FBG stabilization reduces thermal wavelength drift, eliminates chip-to-chip wavelength variations, and enables combination of several pump sources within one single EDFA to provide more pump power.

FBG shows great compatibility with the fiber communication system. Much work has been done in past decades since the invention of FBG [23], [24]. Packaged external fiber grating 1.55-μm semiconductor lasers were reported [25] by BT Laboratories, Ipswich at UK. Operating in single frequency mode, the 1550-nm laser exhibits high output power, high temperature stability operating frequency and low static chirp. Tunable laser with FBG has also been obtained by strain-induced or temperature induced tunable reflection peak of FBG [26].

To achieve successful FBG stabilization of 980-nm LDs, the response of the grating should be broad enough to reflect several longitudinal modes. Therefore the pump laser is operating multimode. The center wavelength of the FBG is chosen to be close to the gain peak to ensure getting as much power as possible. To avoid mode-hopping which occurs at coherent phase, the FBG should be positioned significantly away from the front facet of the laser, beyond the laser coherence length. Therefore FBG locked 980-nm pump lasers work in the coherence collapse operation state.

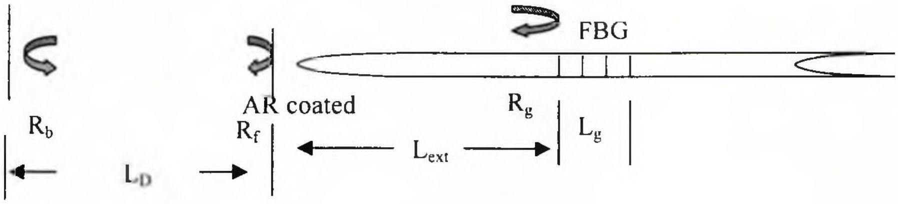

Fig.1.4. Schematic representation of the laser diode and the external fiber Bragg grating

In this thesis, we chose FBG stabilized 980-nm pump laser as the objective to study the partial coherent interaction between the feedback light and the field established in the laser cavity to verify that the interaction is not totally incoherent as normally believed. Coherence collapse has been described by Miles et al [27] and by Goldberg et al [28] in the early 1980's. Daan Lenstra [15] et al noticed that in high feedback level like coherence-collapse, the coherence time τ_{coh} of the output light is much smaller than the external roundtrip time τ. The theory with assumption that the fluctuating phase difference is small for line narrowing explanation does not fit any more. It was argued that, at high feedback levels, the quantum fluctuations (i.e., those associated with spontaneous emission) are completely dominated as a noise driving source by a loss of coherence between the feedback light and the laser light. A self-consistent description of the coherence collapse state was given by usual coupled rate equation model. Theory took the fluctuating phase difference between the delayed feedback field and the laser field inside the cavity as the noise driving force on the phase and intensity fluctuation. In M. Achtenhagen et al [22] they introduced the effective reflectivity R_{eff} by combining the external optical feedback with the front facet reflectivity. Coherence collapse was distinguished with coherent feedback by power reflectivity or by field reflectivity.

In all abovementioned analysis, partial coherent interaction between the feedback light and the field in the laser cavity was not distinguished. D.T. Cassidy reported in 1984 [29] that in the high feedback level, partial incoherence occurs, and the coherently and incoherently interacting feedback light influence the output of the laser in very different fashions. Incoherent feedback light, acting the similar role as spontaneous emission, causes the laser to operate more multimode, while the coherent light causes the laser to operate more single mode. The distinguishing effects can be seen from the difference of quantum slope efficiency derived by light-versus-current (LI) curve. Dr. Cassidy's theory is employed in the feedback effect of FBG-locked 980-nm pump laser in my research. A coherence parameter γ is defined to describe the fraction of feedback light which interacts coherently with the field established in the laser cavity, therefore $0 \leq \gamma \leq 1$. To make sure the pump laser is working in regime IV, the front facet of the laser is AR coated to $R_f \approx 0.04$. The coherence length of the laser light is about 10 mm compared to about 10 m without feedback. In the coherence collapse regime the C parameter is not relevant parameter anymore, since the features of the laser light have become independent of the external cavity length. By changing the external cavity length, the coherence parameter γ will change correspondingly. The coherence parameter can be obtained by the curve of power difference between the L-I curves with and without feedback.

The thesis is organized like this: after the introduction of this chapter, the basic theory of partial coherence describing the interaction between the feedback light and the field in the cavity is reviewed in chapter 2. The coherence parameter γ is introduced in the derivation. In chapter 3, the simulation with traveling-wave method including the effect of nonlinear gain is given. The simulation results will show how the coherence parameter will work on the power difference curve. The measurements setup and results are introduced in chapter 4. Fitting results and analysis are also shown in this chapter. Conclusion is shown in chapter 5.

CHAPTER 2 THEORY

This chapter deals with the theory that lays out the foundation for this thesis. An analytic model of the effects of optical feedback on steady state oscillation spectrum of a diode laser is presented. The feedback light is allowed to interact both coherently and incoherently with the field established in the cavity. The coherence parameter γ is defined in this chapter. A qualitative analysis is given for the effects of coherent and incoherent interaction.

Optical feedback provided by external mirror or grating will alter both the resonant frequency and the intensity of the effects of feedback on the spectral output of semiconductor diode lasers. Much has been published concerning the effects of feedback on the spectral output of diode lasers. But approaches have one drawback in common – all light is assumed to interact totally coherently [5], [10] or totally incoherently [22]. Dr. Cassidy [29] presented that coherent and incoherent interacting feedback light cause very different effect on the oscillation spectrum of the laser. Feedback is included in the laser model by solving the electric fields in a three-mirror Fabry-Perot resonator where one section of the resonator contains a homogeneously broadened gain medium. The model is specialized to the effects which are noticed only on a coarse wavelength scale, which can be observed with a spectrometer, and for distances between the feedback and cavity reflectors which are much greater than the optical length of the laser cavity. The short external cavity is outside of this model because one can reasonably expects all the light to interact coherently

Figure 2.1 is a schematic diagram of a semiconductor laser with an external mirror.

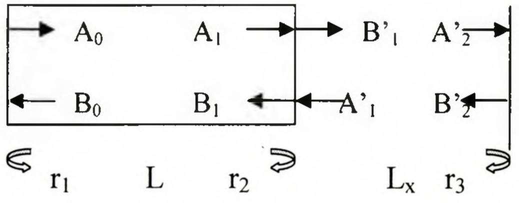

Fig. 2.1 Schematic diagram of a semiconductor laser with an external mirror.

The steady-state of a laser may be modeled by solving for the electric field inside the resonator. The boundary conditions imposed by the cavity reflectors and the single-pass gain supply the relationships between the fields which are required to calculate the output variables in Fig. 2.1 – electric fields at the reflector surfaces. The Fabry-Perot laser has facet amplitude reflection coefficient r_1, r_2 and length L. An external mirror is positioned at a distance L_x away from the front facet of the laser. Note that $L_x >> L$ for this analysis. The external cavity mirror has an amplitude reflection coefficient r_3. The following sets of equations describe the relationships between the electric fields:

$$A_0 = r_1 B_0 \qquad (2.1)$$

$$A_1 = g A_0 e^{j\beta L} + \delta^+ \qquad (2.2)$$

$$B_1^{'} = t_2 A_1 - r_2 A_1^{'} \qquad (2.3)$$

$$A_1^{'} = r_3 B_1^{'} e^{2jkL_x} \qquad (2.4)$$

$$B_1 = t_2 A_1^{'} + r_2 A_1 \qquad (2.5)$$

$$B_0 = g B_1 e^{j\beta L} + \delta^- \qquad (2.6)$$

where δ^+, δ^- denote spontaneous emission coupled to the specific mode, g is the net single-pass gain through the cavity of the laser, $k = 2\pi/\lambda$ and $\beta = n*2\pi/\lambda$ are the wave vectors in the external and laser cavity respectively, t_2 is the transmission coefficient satisfying $t_2^2+r_2^2 = 1$ for lossless mirror.

By defining $r_3^*=r_3e^{2jkLx}$, we rewrite (2.4) as

$$A_1^{'} = r_3^* B_1^{'} \tag{2.7}$$

By substituting Eq. (2.7) into Eq. (2.3), one arrives at

$$B_1^{'} = \frac{t_2}{1+r_2r_3^*}A_1 = t_2^*A_1 \tag{2.8}$$

By defining $t_2^* = \dfrac{t_2}{1+r_2r_3^*}$.

Utilizing Eq. (2.8) and Eq. (2.7), Eq. (2.5) becomes:

$$B_1 = t_2r_3^*B_1^{'} + r_2A_1 = t_2r_3^*t_2^*A_1 + r_{34}A_1 = r_3^{'}A_1 + r_2A_1 \tag{2.9}$$

where $r_3^{'} = t_2r_3^*t_2^*$.

And then Eq. (2.6) may be arranged to eliminate all fields but one

$$B_0 = g^2e^{2j\beta L}(r_3^{'} + r_2)r_1B_0 + g(r_3^{'} + r_2)\delta^+ + \delta^- \tag{2.10}$$

Note that B_0 is the electric field which is traveling in the negative direction and located at the inner surface of back facet. We ignore the phase effect in the spontaneous term in the second step because of the nature of spontaneous emission.

If we assume that a fraction ρ of the field from the feedback mirror 3 interacts completely coherently and 1-ρ interacts completely incoherently, equation (2.10) may be rewritten as:

$$B_0 = g(r_3' + r_2)\delta^+ + \delta^- + g^2 r_1 r_3'(1-\rho)B_0 + g^2(r_2 + \rho r_3')r_1 e^{2j\beta L} B_0 \quad (2.11)$$

Thus the electric field B_0 becomes

$$B_0 = \frac{g(r_3' + r_2)\delta^+ + \delta^- + g^2 r_1 r_3'(1-\rho)B_0}{1 - g^2(r_2 + \rho r_3')r_1 e^{2j\beta L}} \quad (2.12)$$

By distinguishing between coherent and incoherent light we are able to write B_0 in terms of time-dependent and time-independent term. The first two terms in Eq. (2.11) contains contributions from the spontaneous light. As noted by Morrison and Cassidy [53], for Fabry-Perot laser and index-coupled lasers, the cross-correlation (self-interference) effect of the spontaneous photon is negligible. But for the truncated-well gain-coupled DFB lasers, the correlation has to been taken into account for best fits to the below threshold spectra because of the quantum mechanical characteristics of the photon. In our case of Fabry-Perot laser, we believe that it is accurate enough to suppose the phases of δ^+ and δ^- are random in time and uncorrelated. The third term is from the incoherent light, thus it contains a time varying phase and is uncorrelated with the field in the cavity too. The final term in Eq. (2.11) is the correlated term, the phase is defined by the conditions of laser cavity and feedback mirror. Writing $<|B_0|^2> = I^-(\nu)$ as the intensity at back facet, one finds that,

$$I^-(\nu) = \frac{<|\delta|^2>(1 + GR_{eff}) + G^2 R_1 R_3'(1-\gamma)I^-(\nu)}{(1 - G\sqrt{R_1 R_{eff}^{coh}})^2 + 4G\sqrt{R_1 R_{eff}^{coh}}\sin^2(\beta L)} \quad (2.13)$$

where $<|\delta^+|^2> = <|\delta^-|^2> = <|\delta|^2>$ due to the isotropic nature of the gain medium. Here γ is defined as ρ^2 which is the coherent part in intensity of feedback light, $1-\gamma = 1-\rho^2$ is coarsely written as the incoherent part in intensity.

$G = g^2$ is the single-pass gain

$R_1 = |r_1|^2$

$R_3' = |r_3'|^2$

$R_{eff} = |r_2 + r_3'|^2$

$R_{eff}^{coh} = |r_2 + \rho r_3'|^2$

To see clearly the effect of the incoherent part of feedback light, we compare it with an isolated laser. It is well-known that for an isolated laser,

$$I^-(\nu) = \frac{<|\delta|^2> (1 + R_2 G)}{(1 - G\sqrt{R_1 R_2})^2 + 4\sqrt{R_1 R_2} G \sin^2(\beta L)} \tag{2.14}$$

Equation (2.14) indicates that a laser operates as a resonance amplifier of spontaneous emission. It is shown in Eq. (2.13) that the fraction of feedback light which interacts incoherently with the field in the cavity acts as the same role of spontaneous emission. The light which interacts coherently increases the reflectivity of the front facet by changing R_2 to R_{eff}^{coh}. Thus only the coherent fraction of feedback light works to increase the slope efficiency.

Cassidy noted that the two forms of feedback, coherent and incoherent, tend to cause competing effects to the spectral output of the laser. Light feedback into the laser which is incoherent with the field in the cavity is working as the similar way as spontaneous light. The incoherent light will experience more gain than spontaneous light because its spectral profile is same as the mode. Therefore the laser is sensitive to incoherent feedback. The effect of the incoherent feedback light is to cause the laser to operate more multimode than it would without the feedback of incoherent light. In contrast, the coherent feedback light effectively increases the facet reflectivity. By reducing the threshold of the dominant lasing mode, the adjacent modes which exhibit a higher threshold gain will be suppressed [9]. The coherent feedback light causes a more single-mode operation.

The coherence parameter γ plays a critical role in discriminating the different effects of coherent and incoherent feedback light. When γ equals to 1, all the feedback light is supposed to interact coherently, and $\gamma = 0$ corresponds to all the feedback light interacting incoherently, $0 < \gamma < 1$ is the state of partial coherence. In paper [29], Dr. Cassidy noted that the coherence parameter γ can be figured out by the difference in the output power with and without feedback as a function of the pumping rate. Figure 2.2 shows the computer-generated plots of optical power at back facet of the 980 nm pump laser with mirror as an external cavity.

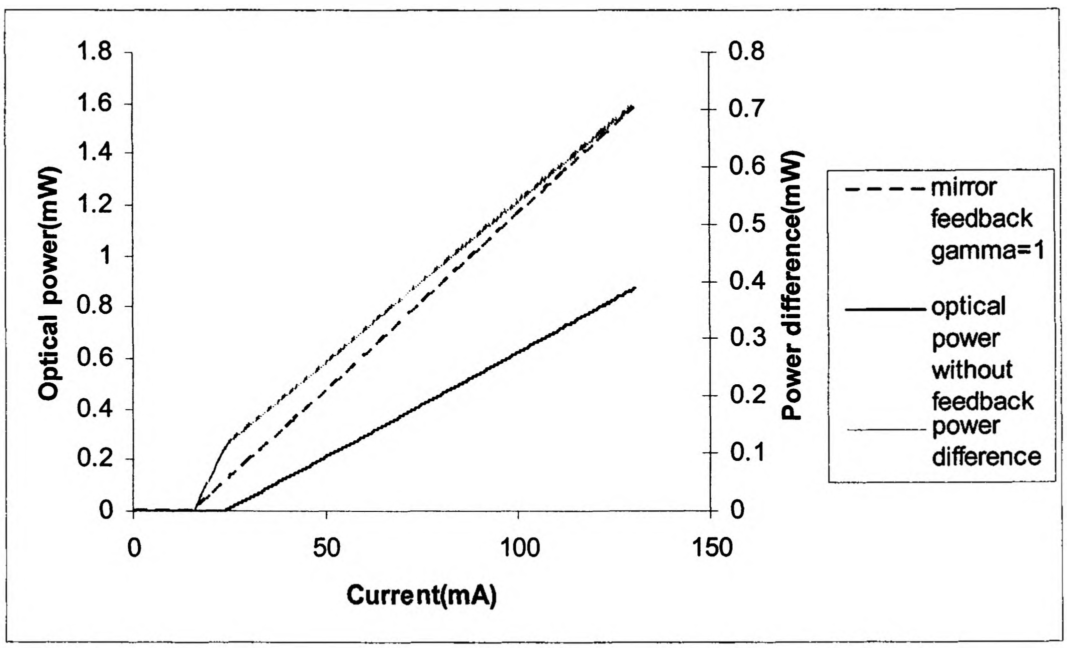

(a)

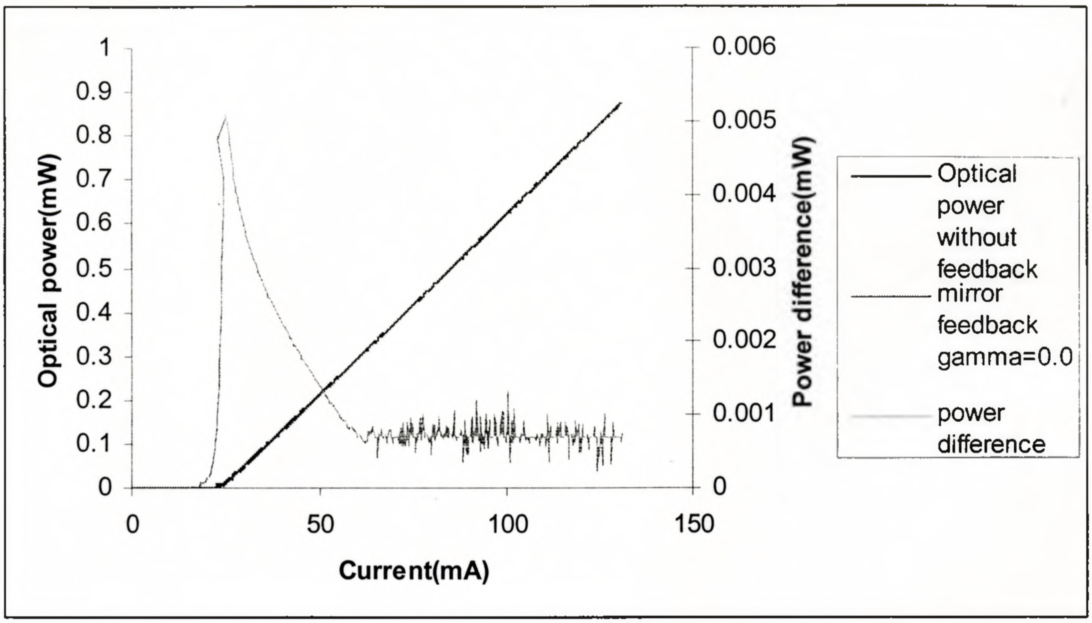

(b)

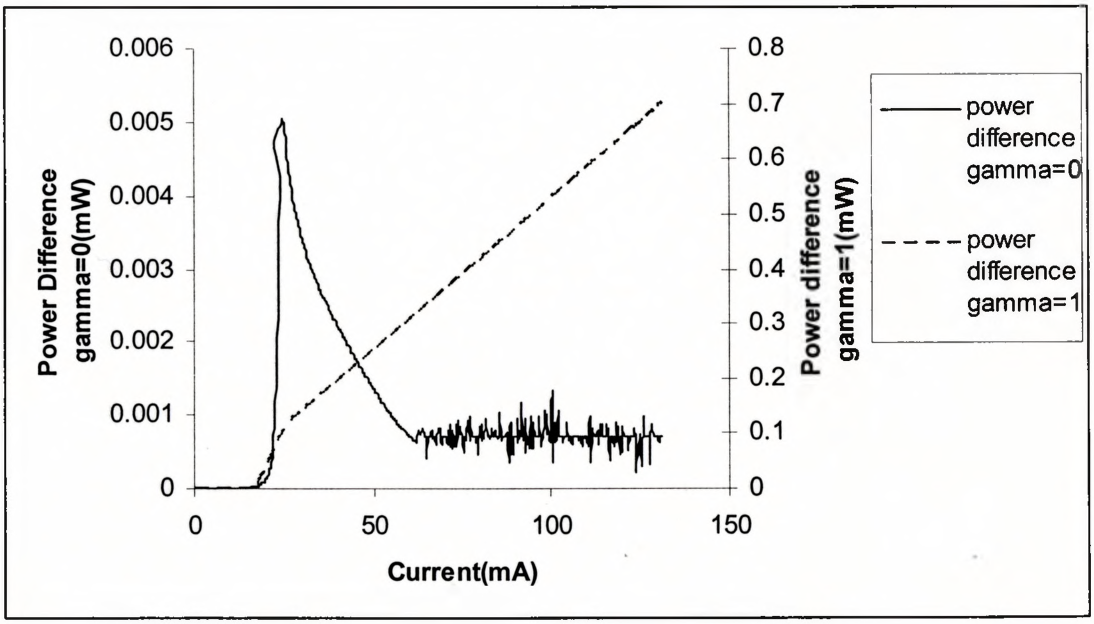

(c)

Fig.2.2. (a) plot of total output power at back facet without feedback, with totally coherent feedback, and the power difference between them as a function of injected current.(b) plot of total output power at back facet without feedback, with totally incoherent feedback, and the power difference.(c) comparison of power difference under totally coherent and totally incoherent feedback.

Figure 2.2 (a) was calculated assuming that all the feedback light interacts coherently. Figure 2.2 (b) was calculated assuming that all the feedback light interacts incoherently. To see it clearly, the output power without feedback as a function of current at the same facet are also shown in the figures. It is shown that the coherent and incoherent feedback light cause drastically different effect on the total output power of the laser. Both the coherent feedback light and incoherent light reduce the threshold current. However, the coherent feedback increases the output power above threshold by raising the slope efficiency and causes the difference in power to be a linear function of the pumping rate. The incoherent feedback light increases the output power very rapidly just-above threshold and far-above threshold the incoherent feedback increases the power by an amount which is approximately independent of the pumping rate.

To see the effect on the laser spectrum, I show in Fig. 2.3 the computer generated plots of total optical output power and modes' power for a laser with mirror feedback. Nine modes are calculated in the simulation. Figure 2.3 (a) was generated under the assumption that all the feedback light is incoherent, in which it is shown that the laser is running multimode above threshold. Figure 2.3 (b) was generated under the assumption that all the feedback light is coherent. It is clear that the laser is running mostly in mode 0 and mode 1 above threshold, and most of the power is focused in the main mode, a large SMSR is obtained in this case.

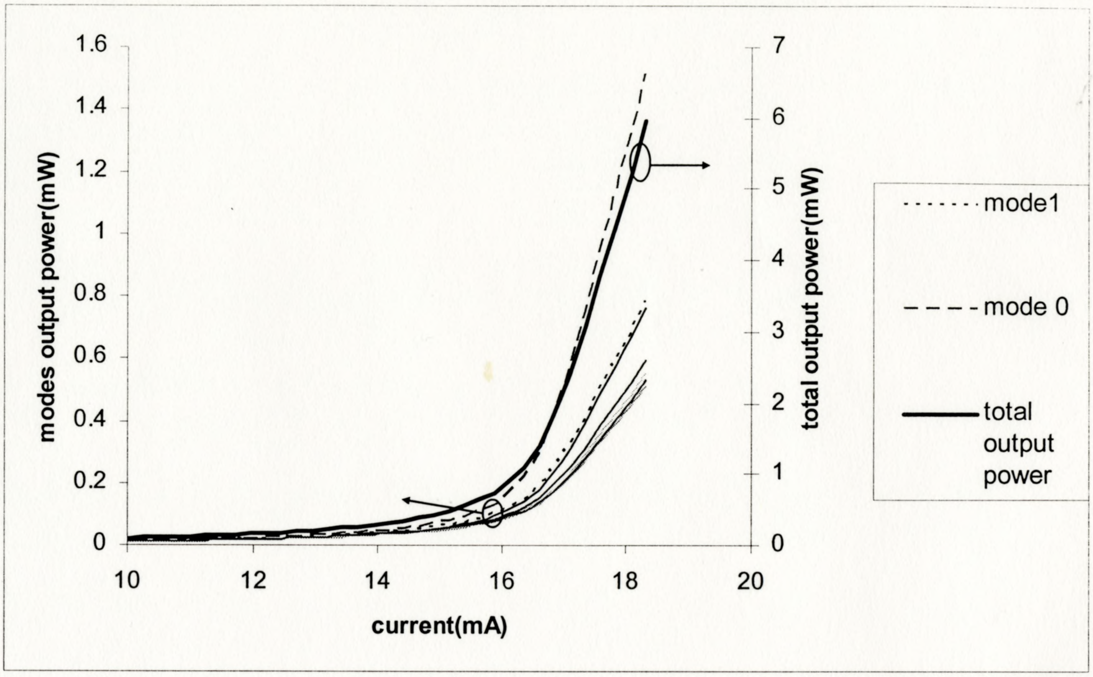

1.6
1.4
1.2
1
0.8
0.6
0.4
0.2
0
7
6
5
4
3
2
1
0
10
12
14
16
18
20
current(mA)
modes output power(mW)
total output power(mW)
mode1
mode 0
total output power

(a)

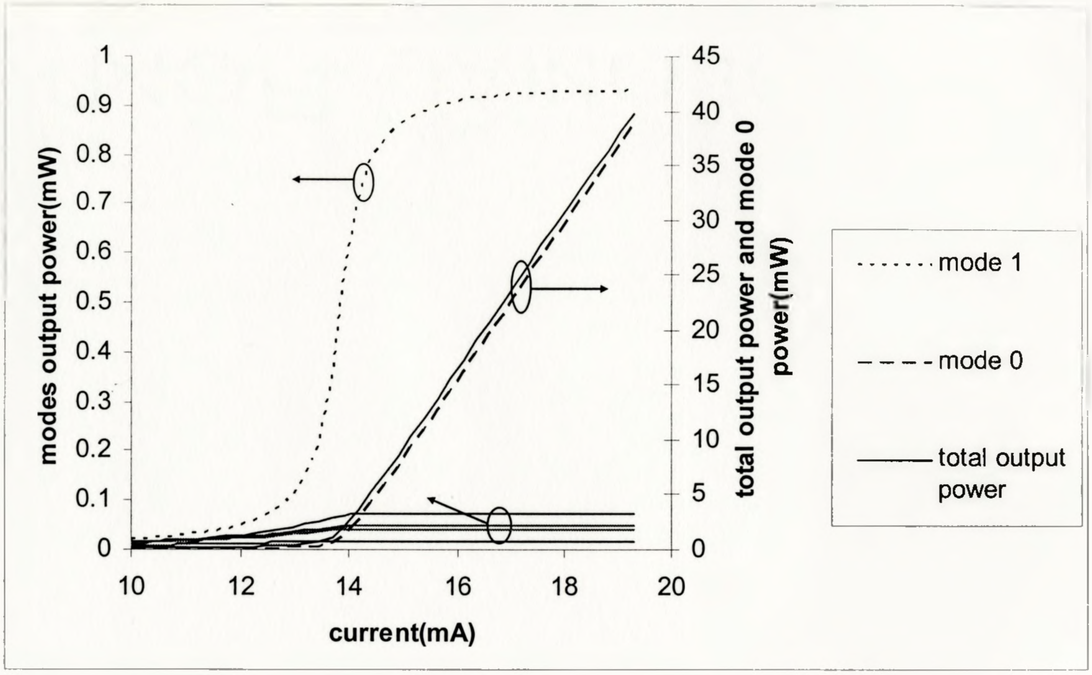

(b)

Fig. 2.3 Computer-generated plots of the total output power and the power in nine modes near the gain peaks as a function of injection current. (a) all light interacting incoherently ($\gamma = 0$); (b) all light interacting coherently ($\gamma = 1$)

Based on this theory, I worked on 980-nm pump laser with FBG wavelength stabilization which works in the regime of "coherence-collapse". Since the coherence length L_c is much smaller than the external cavity length L_{ext}, the partial coherent interaction was applied. By moving the FBG further away or closer to the front facet of the laser, the coherence parameter γ which determines the fraction of feedback interacting coherently will change correspondingly. We expected that the shorter the external cavity, the higher the coherence parameter should be. In chapter 3, simulation with traveling wave method based on Dr. Cassidy's theory is given. By fitting the power difference curve to the measurement results, which are shown in chapter 4, the coherence parameter γ is figured out, so is the scale of feedback which coherently interacts with the field in the laser cavity. I'll also show in chapter 4 that by changing the amount of feedback with a neutral-density (ND) filter, (in this case the laser is still working in the coherence collapse regime), the coherence parameter γ would not change. This agrees with the other works [14], [30], [31] on coherence collapse which concludes that the linewidth of the laser would not change much in the whole range of coherence collapse from -40 dB to -10 dB.

CHAPTER 3 SIMULATION

As discussed in chapter 2, the coherence parameter γ denotes the fraction of feedback light which interacts coherently with the field in the laser cavity. It can be embodied in the light-current (L-I) curve. In this work, the shape of the power difference with pumping, which is introduced by the external cavity, is used to determine the value of γ. The slope efficiency of the power difference versus current curve changes with the coherence parameter. The larger the slope efficiency, the bigger is the coherence parameter. In this chapter, modeling of partially coherent interaction of feedback light in the steady state is introduced through FBG stabilized 980-nm pump laser. The effective wavelength-dependent reflectivity method was adopted in the model. We applied Fabry-Perot approach (traveling wave model) other than rate-equation model because it is more accurate for an asymmetric laser cavity. The effective reflectivity of the front facet R_{eff} is derived in section 3.1. Fiber Bragg grating reflection accompanied with the phase delay and finite bandwidth cause the effective reflectivity to be complex and wavelength dependent. The FBG reflectivity is shown in section 3.2. The incoherent fraction of feedback light works as the additional spontaneous emission which is applied to the last section of the laser cavity, and will experience coherent amplification while bouncing back and forth in the cavity. A second-order Runge-Kutta method was used to solve the differential equations.

3.1 Effective reflectivity

In the following, we consider a laser and FBG stabilized module, as described schematically in Fig. 3.1.

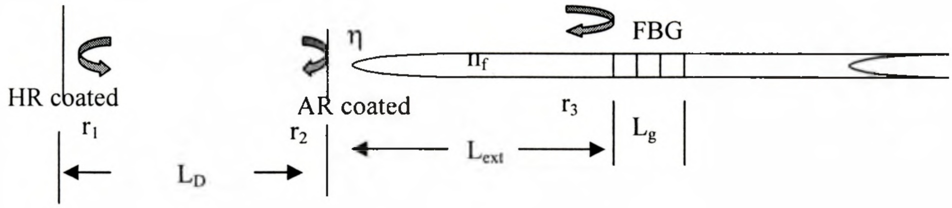

Fig. 3.1 Schematic representation of the laser diode and the external fiber Bragg grating

It is a typical active-passive coupled-cavity scheme. Here a diode laser, represented by an active medium of length L_D with plane mirrors, is coupled to a tapered single-mode fiber. The fiber is corning HI 1060 single mode fiber with mode field diameter 5.9 μm at 980 nm wavelength and was tapered at the end to increase the coupling efficiency. The single mode fiber with a Bragg grating located about 2 meters away works as the external cavity. The amplitude reflectivity of the laser facets are r_1 and r_2 for the back and front facet respectively. The facets are assumed to be lossless such that $r_2^2+t_2^2=1$, where t is the transmission. The front facet is normally AR coated to about 4%, the back facet is HR coated to 93%. The reflectivity of the FBG, which is represented by r_3, is wavelength dependent and complex because it will introduce phase delay according to specific wavelength. The refractive indices of the active medium and the single mode fiber are n_c and n_f respectively.

Usually, the coupled-cavity configuration is analyzed as a simple two-mirror laser structure by replacing the diode laser output facet reflectivity r_2 by a complex-valued effective amplitude reflection coefficient $r_{eff}(\omega)$, which takes into account the effects of both r_2 and $r_3(\omega)$. This works for the short external cavity. However, in the case of "coherence-collapse", we have to consider the coherence parameter γ because not all of the returned light is coherent. To see it clearly, we plot the external cavity in Fig. 3.2 which replaces the fiber with medium n_f and the FBG with a mirror $r_{fbg}(\omega)$.

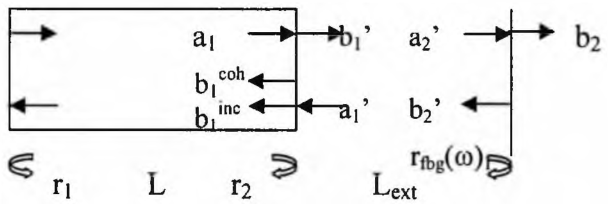

Fig. 3.2 External cavity for derivation of $r_{eff}^{coh}(\omega)$

The relationships between the electric fields shown in Fig. 3.2 are written in the following (all the fields are supposed to be in the same polarization).

$$b_1^{coh} = r_2 a_1 + a_1' t_2 \sqrt{\gamma} \qquad (3.1)$$

$$b_1' = a_1 t_2 - a_1' r_2 \qquad (3.2)$$

$$b_2 = a_2' t_{fbg}(\omega) \qquad (3.3)$$

$$b_2' = a_2' r_{fbg}(\omega) \qquad (3.4)$$

$$a_1' = b_2' e^{-j\beta L_{ext}} \eta \qquad (3.5)$$

$$a_2' = b_1' e^{-j\beta L_{ext}} \eta \qquad (3.6)$$

Equation (3.1) through (3.6) may be interpreted as that the electric field b_1 at the surface of r_2 and traveling in the positive direction is the fraction r_2 of the electric field a_1 plus the transmission coherent part of a_1' which is fed back from the external cavity mirror. Note that $\sqrt{\gamma}$ appearing here because we defined the coherence parameter as the power fraction. The field $b_1^{'}$ traveling in positive direction is composed by the transmission fraction of a_1 and reflection fraction of the feedback light $a_1^{'}$. The field $b_2^{'}$ is related to the incident electric field by the complex FBG reflector $r_{fbg}(\omega)$. The reflectivity of FBG will be described in next section. The field $a_1^{'}$ in the negative direction at surface r_2 is related to the field $b_2^{'}$ by a phase change $\exp(-j\beta L_{ext})$ from propagating over a distance L_{ext} where $\beta = n_f k$. n_f is the effective index of fundamental mode of the fiber. Coupling efficiency η is multiplied here which is normally 30%~50%. From this discussion the definition of all the terms in Eq. (3.1~3.6) should be apparent.

The effective reflectivity for the passive section as viewed from the active section is $r_{eff}^{coh} = b_1/a_1$.

Substitute Eq. (3.5) into Eq. (3.1), we get

$$b_1^{coh} = r_2 a_1 + b_2^{'} e^{-j\beta L_{ext}} \eta t_2 \sqrt{\gamma} \tag{3.7}$$

with $b_2^{'} = a_2^{'} r_{fbg}(\omega)$ and Eq. (3.6), Eq. (3.7) becomes

$$b_1^{coh} = r_2 a_1 + (a_1 t_2 - \frac{b_1 - r_2 a_1}{t_2 \sqrt{\gamma}} r_2) e^{-2j\beta L_{ext}} \eta^2 r_{fbg}(\omega) t_2 \sqrt{\gamma} \tag{3.8}$$

Reorganizing Eq. (3.8), finally we get,

$$r_{eff}^{coh}(\omega) = \frac{b_1^{coh}(\omega)}{a_1} = r_2 + \frac{t_2^2 \eta^2 r_{fbg}(\omega) e^{-2j\beta L_{ext}} \sqrt{\gamma}}{1 + \eta^2 r_2 r_{fbg}(\omega) e^{-2j\beta L_{ext}}} \tag{3.9}$$

Now the effect of coherent fraction of feedback light is clearly demonstrated. The increase of front facet reflectivity is caused only by the coherent part, not by the incoherent part. This will be connected to the increase of the quantum efficiency of the laser. On the other hand, to see the effect of incoherent interaction, we write it as:

$$b_1^{inc} = \sqrt{1-\gamma}\, a_1^{'} t_2 \tag{3.10}$$

Combining Eq. (3.10) with Eq. (3.2~6) and following the similar routine as we derive r_{eff}^{coh}, we obtain:

$$b_1^{inc}(\omega) = \frac{a_1\sqrt{1-\gamma t_2^2}\,\eta\,|\,r_{fbg}(\omega)\,|}{1+r_2\,|\,r_{fbg}(\omega)\,|\,\eta^2} \tag{3.12}$$

In deriving Eq. (3.12), note that because b_1^{inc} works as spontaneous emission, it has no consistent phase correlation to the field in the cavity. So the time average of the phase relation should be zero.

The incoherent field $b_1^{inc}(\omega)$ works as noise at the front end of the laser cavity. The difference between $b_1^{inc}(\omega)$ and spontaneous emission is that $b_1^{inc}(\omega)$ is added to specific modes where it exists, however the spontaneous emission is uniformly distributed in wavelength over an interval corresponding to the free spectral range of the laser. Only the light in spontaneous emission that has the same range of frequency and detection as the longitudinal modes will be resonantly amplified by the laser cavity. The feedback light, in contrast, is distributed over an interval corresponding to the linewidth of the laser. Thus a small amount of incoherent feedback light will cause the laser to run more multimode than spontaneous emission does.

3.2 Fiber Bragg grating (FBG) reflection spectrum

3.2.1 Introduction to fiber gratings

First discovered by Ken Hill and his co-workers at the Communication Research Center (CRC) in Ottawa [32], the fiber phase grating has developed into a critical component for many applications in fiber-optic communication and sensor systems. A fiber grating is fabricated by writing ultraviolet light into the core of an optical fiber which has a photosensitivity. Fiber gratings can be broadly classified into two types: fiber Bragg grating (short period grating) in which coupling occurs between modes traveling in opposite directions, and transmission gratings (long period gratings), in which the coupling is between modes traveling in the same directions. In the works of this thesis, we are using the fiber Bragg gratings.

Fabrication techniques of FBG broadly fall into two categories: holographic method [33] and phase mask method [34]. The former technique uses a beam splitter to divide a single input UV beam into two, interfering them at the fiber. The latter depends on periodic exposure of a fiber through a spatially periodic surface relief (phase mask). The phase-mask method is thought to be one of the best techniques for mass fabrication of the fiber Bragg grating because of easy alignment, reduced requirements for stability of the system and coherence of the UV laser beam, and flexibility of the process for writing varieties of gratings. Much work has been done on the optimization of phase masks for FBG fabrication [35] and diffractive optics of the phase mask with fabrication error introduced by E-beam etching [36], [37].

Advantages of fiber gratings over competing technologies include all-fiber geometry, low insertion loss, high return loss or extinction and low loss. However, the most distinguishing feature of fiber grating is the flexibility it offers for achieving desired spectral characteristics. Numerous physical parameters can be varied including: induced index change, length, apodization, period chirp and fringe tilt. By varying these parameters, gratings can be made with normalized bandwidths ($\Delta\lambda/\lambda$) between 10^{-1}~10^{-4}, i.e., with extremely sharp spectral features and tailorable dispersive characteristics. The applications of the fiber gratings include: WDM, narrow and broadband fiber filters, dispersion compensation [38], EDFA gain flattening and fiber sensor. The application of FBG in the 980-nm pump laser uses the Bragg reflection characteristic. The reflection spectra of FBG are introduced in next section.

3.2.2 FBG spectra [39]

For simplicity, the perturbation to the effective refractive index n_{eff} of the guide modes in the fiber can be described by:

$$\delta n_{eff}(z) = \overline{\delta n_{eff}}(z)\{1 + v\cos[\frac{2\pi}{\lambda}z + \phi(z)]\} \tag{3.13}$$

where $\overline{\delta n_{eff}}$ is the "dc" index change spatially averaged over a grating period, υ is the fringe visibility of the index change, Λ is the nominal period, and $\phi(z)$ describes the grating chirp. If the fiber has a step-index profile and an induced change $\delta n_{co}(z)$ is created uniformly across the core, then we find that $\delta n_{eff} \cong \Gamma\delta n_{co}$, where Γ is the core power confinement factor for the mode of interest. When the light wave in the fiber is incident on the gratings, only those wavelengths which satisfy the Bragg condition will be reflected efficiently:

$$\beta_2 = \beta_1 + m\frac{2\pi}{\Lambda} \tag{3.14}$$

where β is the mode propagation constant ($\beta = n_{eff}2\pi/\lambda$). β_1 and β_2 denote the forward and backward propagating mode in an FBG and β is negative when describing modes that are propagating in the negative z direction. m determines the diffraction order, and for first-order diffraction m = -1. For the two modes which are identical but in opposite direction, we get the familiar result for Bragg reflection,

$$\lambda = 2n_{eff}\Lambda \tag{3.15}$$

Coupled-mode theory [39] is the basic tool for obtaining quantitative information about the diffraction efficiency and spectral dependence of fiber gratings. For arbitrary or non-uniform gratings, the coupling occurs predominantly between two modes. There is an analytical solution only for the uniform FBG. Numerical solution such as adaptive step size Runge-Kutta method has to be applied for calculating the reflection and transmission spectra for non-uniform gratings. The FBG we used in this thesis work is the uniform and single mode Bragg grating. The reflection FBG spectrum is introduced in the following. Figure 3.3 shows the ray-optic illustration of core-mode Bragg reflection by a fiber Bragg grating.

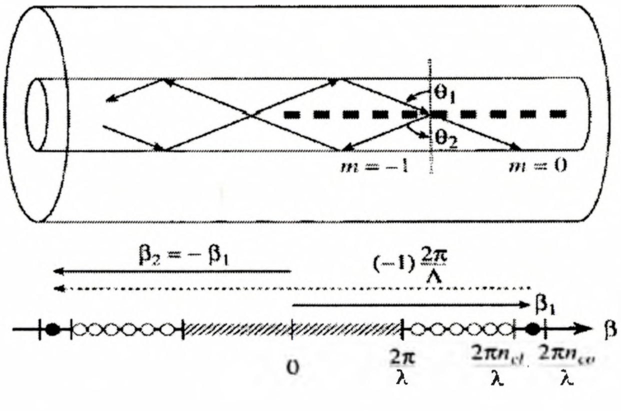

Fig. 3.3 Ray-optic illustration of core-mode Bragg reflection by a fiber Bragg grating

The couple-mode equations are given as:

$$\frac{dR}{dz} = i\hat{\sigma}R(z) + i\kappa S(z) \tag{3.16}$$

$$\frac{dS}{dz} = -i\hat{\sigma}S(z) - i\kappa^* R(z) \tag{3.17}$$

where $R(z) \equiv A(z)e^{i\delta z - \frac{\phi}{2}}$ is the mode traveling in the +z direction and $S(z) \equiv B(z)e^{-i\delta z + \frac{\phi}{2}}$ is the mode traveling in the –z direction, A(z) and B(z) are the amplitude respectively. The detuning factor δ, which is defined as the frequency difference from the designed wavelength, is given as:

$$\delta \equiv \beta - \frac{\pi}{\Lambda} = \beta - \beta_D = 2\pi n_{eff}(\frac{1}{\lambda} - \frac{1}{\lambda_D}) \tag{3.18}$$

where $\lambda_D = 2n_{eff}\Lambda$ as shown in Eq. (3.15). Note when $\delta = 0$, we get to $\lambda = 2n_{eff}\Lambda$, the Bragg condition is satisfied. $\hat{\sigma}$ is a general "dc" self coupling coefficient defined as

$$\hat{\sigma} \equiv \delta + \sigma - \frac{1}{2}\frac{d\phi}{dz} \tag{3.19}$$

where σ is a "dc"(period averaged) coupling coefficient, given by:

$$\sigma(z) = \frac{\omega n_{eff}}{2}\overline{\delta n_{eff}}(z) \iint_{core} dxdy\vec{e}_{1t}(x,y)\vec{e}_{1t}^{\,*}(x.y) \tag{3.20}$$

and κ in Eq. (3.16)(3.17) is the coupling coefficient defined as:

$$\kappa = \frac{v}{2}\sigma \tag{3.21}$$

Note that $\frac{1}{2}\frac{d\phi}{dz}$ in Eq. (3.19) and the coupled-mode equations describe a possible chirp of the grating period. In the case of uniform grating, it turns to be zero. Among the parameters shown above, κ is the most important one. It shows how strongly the forward and backward propagation modes are coupled.

For a single-mode Bragg reflection grating there exits the following relations:

$$\sigma = \frac{2\pi}{\lambda}\overline{\delta n_{eff}} \tag{3.22}$$

$$\kappa = \kappa^* = \frac{\pi}{\lambda}v\overline{\delta n_{eff}} \tag{3.23}$$

If the grating is uniform along z, then δn_{eff} is a constant, R, σ and $\hat{\sigma}$ are constants. Thus Eq. (3.16) and Eq. (3.17) are coupled first-order ordinary differential equations with constant coefficients. A closed form solution can be found with appropriate boundary conditions.

The reflectivity of a uniform fiber grating of length L can be found by assuming R(-L/2) = 1 and S(L/2) = 0, requiring that a forward-going wave incident from z = -∞, and no backward-going wave exist for z ≥ L/2. The complex amplitude reflection coefficient $r_{fbg}(\omega)$:

$$r_{fbg}(\omega) = \frac{-\kappa\sinh(\sqrt{\kappa^2-\hat{\sigma}^2}L)}{\hat{\sigma}\sinh(\sqrt{\kappa^2-\hat{\sigma}^2}L)+i\sqrt{\kappa^2-\hat{\sigma}^2}\cosh(\sqrt{\kappa^2-\hat{\sigma}^2}L)} \tag{3.24}$$

The power reflection coefficient $R_{fbg} = |r_{fbg}|^2$ is:

$$R_{fbg} = \frac{\sinh^2(\sqrt{\kappa^2-\hat{\sigma}^2}L)}{\cosh^2(\sqrt{\kappa^2-\hat{\sigma}^2}L)-\frac{\hat{\sigma}^2}{\kappa^2}} \tag{3.25}$$

Figure 3.4 shows the amplitude reflection and the phase retardation of FBG respectively which is used in wavelength stability of 980-nm pump laser. The central wavelength is $\lambda_{max} = 977.8$ nm at which maximum reflectivity occurs. In the case we used in the experiment R_{max} is about 4%. The parameters applied in the simulation of Fig. 3.4 and 3.5 are shown in Table 3.1.

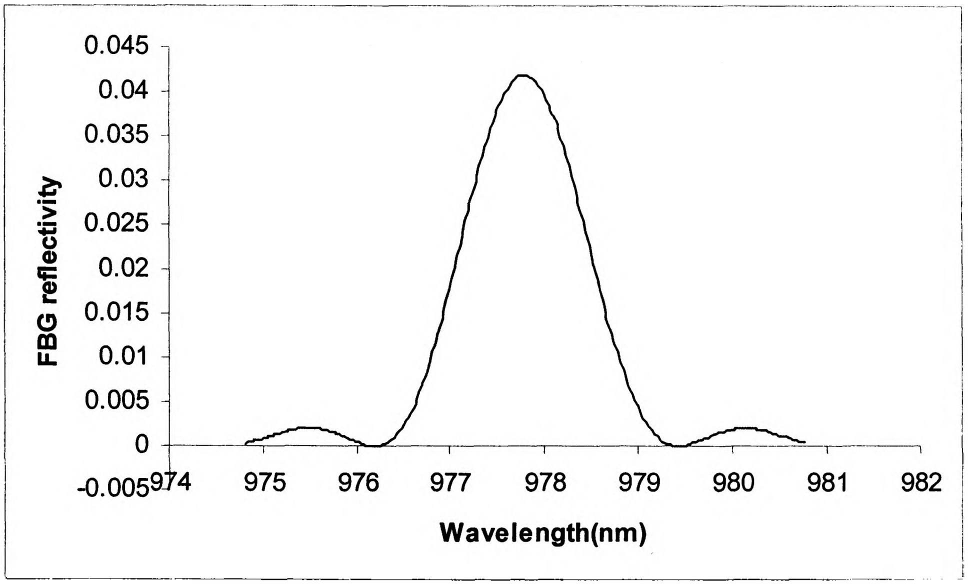

Fig. 3.4 Reflection spectra versus wavelength for FBG reflection in uniform grating with $\kappa L = 0.208$

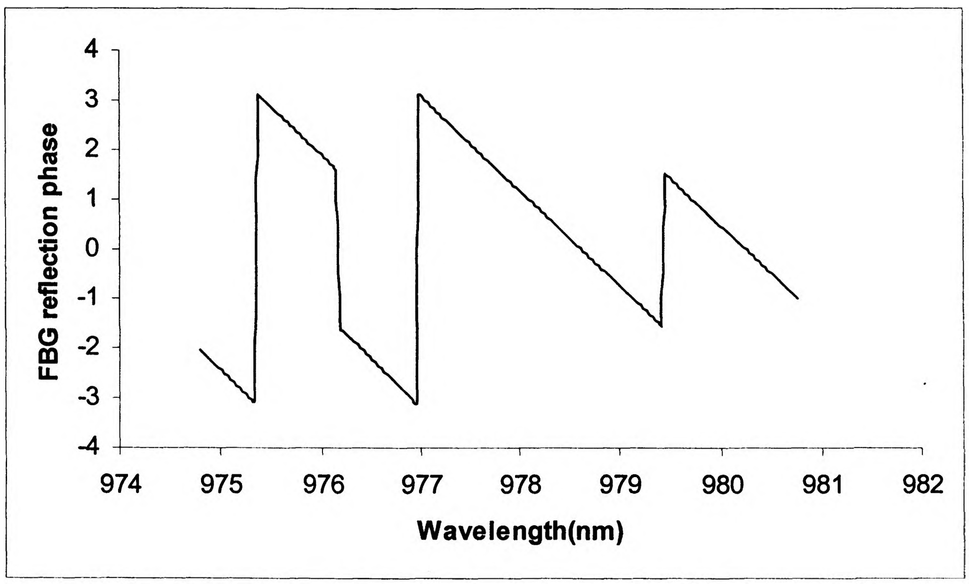

Fig. 3.5 Reflection phase spectra of FBG reflection in uniform grating with $\kappa L = 0.208$

Table 3.1 Parameters values used for FBG reflection spectrum simulations

fiber effective refractive index	n_{eff}	1.44783
fiber grating length	L	0.2028 mm
AC refractive index change	δn_{eff}	3.186×10^{-4}
design wavelength	λ_D	977.58 nm
grating period	Λ	337.6 nm
central wavelength	λ_{max}	977.80 nm
coupling coefficient	$\kappa = \frac{\pi}{\lambda} v \overline{\delta n_{eff}}$	
Visibility	v	1

3.3. Phase condition for longitudinal mode selection

The standard requirement for steady state operation of a solitary laser with facet reflectivity of r_1 and r_2 is written as:

$$r_1 r_2 e^{gL-2jkL} = 1 \tag{3.26}$$

In the effective reflectivity model of a laser with external cavity, Eq. (3.26) turns to:

$$r_1 r_{eff}^{coh}(\nu) e^{gL-2jkL} = 1 \tag{3.27}$$

where $r_{eff}^{coh}(\nu)$ is complex, can be written as,

$$r_{eff}^{coh}(\nu) = | r_{eff}^{coh}(\nu) | e^{-j\phi_{eff}^{coh}(\nu)} \tag{3.28}$$

Equation (3.27) can be separated into the usual phase and gain conditions for steady state operation

$$r_1 \,|\, r_{eff}^{coh}(\nu) \,|\, e^{gL} = 1 \qquad \text{(gain condition)} \qquad (3.29)$$

$$\phi_L = 2kL + \phi_{eff}^{coh}(\nu) = 2m\pi \qquad \text{m integer} \qquad \text{(phase condition)} \qquad (3.30)$$

where $k = n_c 2\pi/\lambda$. In the case of FBG feedback, the longitudinal modes would be chosen numerically according to the phase delay of both fiber and FBG using Eq. (3.9) by substituting Eq. (3.24) in it.

3.4 Fabry-Perot model (traveling wave model)

3.4.1 Fabry-Perot model vs. rate-equation model

Two approaches to modeling the steady state light-versus-pumping characteristic of diode lasers are normally exploited. Cassidy noted in his work in 1983 [40] that Fabry-Perot (F-P) approach is more accurate than rate equation model in two factors: first, the F-P model explicitly includes the resonator, whereas in the rate-equation description the cavity is included by defining an effective loss α. Second, for the Fabry-Perot approach, allowing for the other forms of gain and distributed nature of the spontaneous light are automatically included. It was noted that modification to rate equations should be done in three aspects: a scaled pumping rate, an effective spontaneous emission factor $\beta' = \beta(1+\alpha'/2)$, and a cavity loss $\alpha = 1 - R + \alpha'$. Furthermore, the rate equation description is valid only for small gain coefficients and absorption/scattering loss α' so that the exponential function for $G_m = \exp(ng_m - \alpha')$ can be expanded with Taylor series where only linear terms are retained. The exponential gain causes the distribution of energy among the modes to be different than for the linear gain, although the total-power-versus-pumping characteristics can be similar by two models. It was verified by the single-pass gain G versus pumping rate curve that the traveling wave solution of FP model should be preferred to modeling a diode laser.

3.4.2 Traveling wave solution

The following equations were used to describe the amplification of the modes and the population inversion n(x) in an infinitesimal of gain material in the cavity.

$$\frac{dn(x)}{dt} = pump - An(x) - Bn^2(x) - Cn^3(x) - \sum_{i=1}^{N_{modes}} g_i n(x)(I_i^+ + I_i^-) \tag{3.30}$$

$$\frac{dI_i^\pm(x)}{dx} = \pm g_i n(x) I_i^\pm(x) + \frac{\beta B n^2(x)}{N_{modes}} \tag{3.31}$$

$$\frac{dG_i}{dx} = g_i n(x) G_i \tag{3.32}$$

The meanings of variables are defined in Table 3.2

Table 3.2 Parameter definitions in Eq.(3.30-32)

$n(x)$	Population inversion at position x in the cavity ($/cm^3$)
pump	pumping rate ($/cm^3/s$)
A	Nonradiative coefficient (/s)
B	Radiative coefficient (cm^3/s)
C	Auger coefficient (cm^6/s)
g_i	The differential gain coefficient of mode I (cm^2)
$I_i^{\pm}(x)$	The photon numbers in mode i for travelling in + or – directions ($/cm^2/s$)
N_{modes}	The number of longitudinal modes
β	The spontaneous emission factor
G_i	The single-pass gain of mode i

Equation (3.30) describes the rate of change of population inversion in terms of pumping rate "*pump*", spontaneous emission, nonradiation combination, and stimulated emission. In steady state, it goes to $dn(x)/dt = 0$ to solve for the inversion population at certain injected current. Equation (3.31) illustrates that the optical intensity will experience an increment after propagating through an infinitesimal thickness of gain material dx in positive and negative direction by the stimulated emission and the fraction β of spontaneous emission which is coupled to mode i. Equation (3.32) demonstrates the relation of single-pass gain to inversion population and thus to the pumping rate. Note that exponential gain is allowed in this model. g_i, the differential gain coefficient, was obtained through measuring the emission spectra of the laser [41]. Spectral hole burning

[44] was taken into account for the reason that the 980-nm pump laser works in the high power regime. The measurement of gain spectrum is shown in the next section.

A second order Runge-Kutta technique was used to solve numerically the differential equations. The steady state solutions can be found by applying boundary conditions of optical fields at both the back and front facets of laser cavity. As shown in Fig. 3.6, boundary conditions are $I^+(0) = I^-(0)R_b$, and $I^-(L) = I^+(L)R_{eff}^{coh}(\nu)$, where $R_{eff}^{coh}(\nu) = |r_{eff}^{coh}(\nu)|^2$

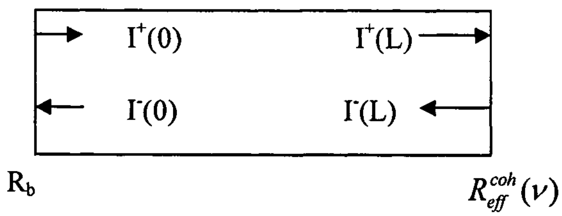

Fig. 3.6 Boundary condition for laser model

The flow chart for traveling wave solution is given in Fig. 3.7. The initial guess for the optical power at the beginning of pumping rate (k = 1) is normally the spontaneous emission appearing in Eq. (3.31). The new guess for next pumping rate (k = k+1) is based on the optical power obtained by former steps by extrapolation.

The second-order Runge-Kutta method is an approach that changes the task from performing a differential equation as dy/dx = f(x,y) to an integral equation:

$$y_{n+1} = y_n + hf(x_n + \frac{h}{2}, y_n + \frac{k}{2}) \qquad (3.33)$$

$$k = hf(x_n, y_n) \qquad (3.34)$$

$f(x_n, y_n)$ is the right hand of Eq. (3.12). h is the step distance and has an unit of length in our case.

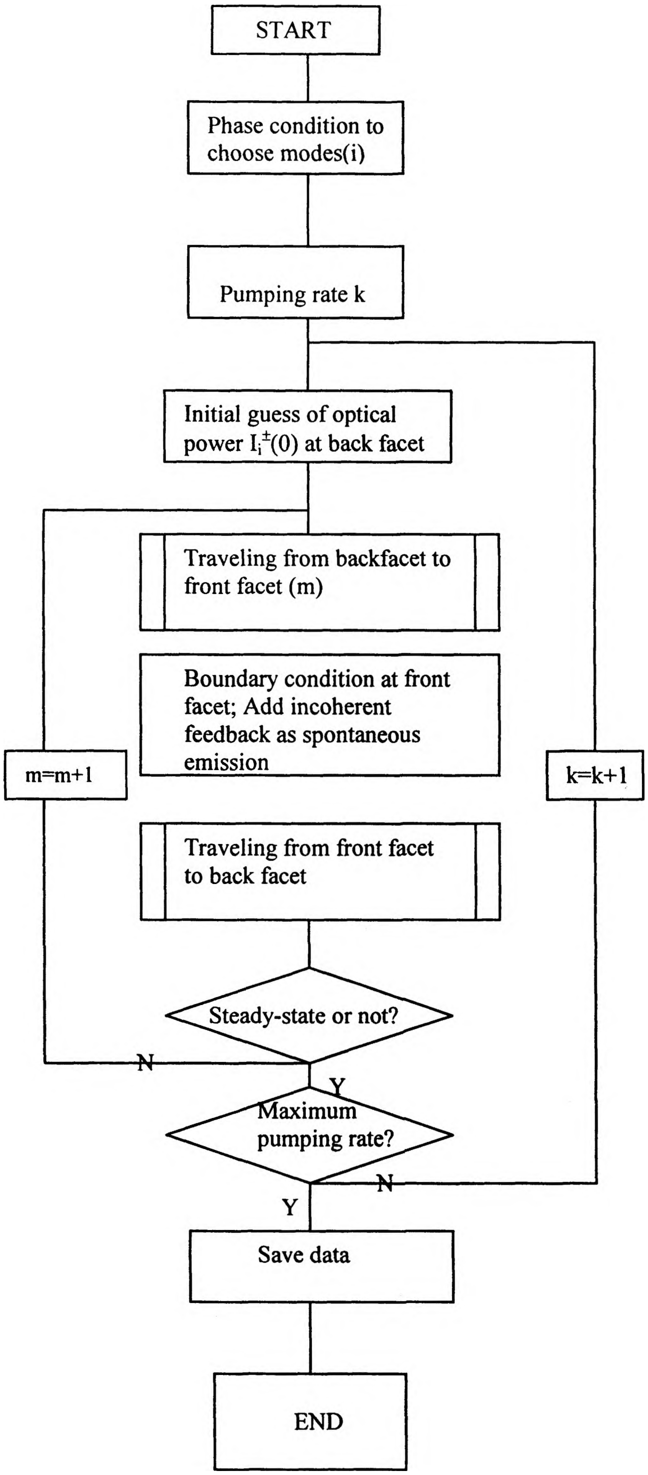

Fig. 3.7 Flow chart of traveling wave method for simulation of FBG stabilized 980-nm pump laser in steady state

Combined with second-order Runge-Kutta method, the step shown by double line in the flow chart as "traveling from back facet to front facet" and "traveling from front facet to back facet" could be interpreted as Fig. (3.8).

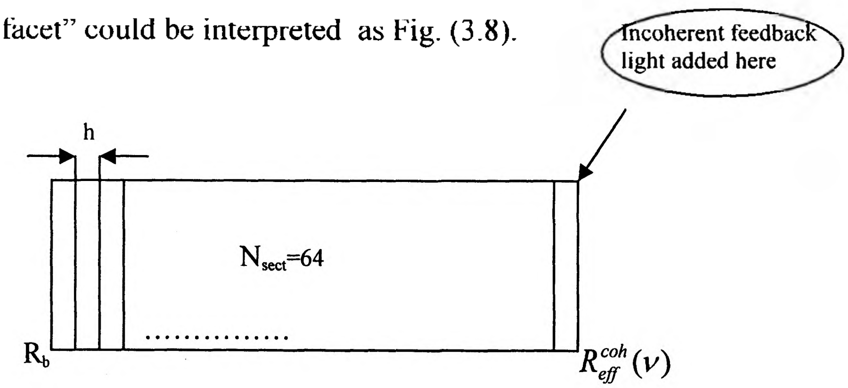

Fig. 3.8 Traveling wave method by Runge-Kutta method

The laser cavity is divided in $N_{sects} = 64$ number of sections for solution of Runge-Kutta method. We start with the initial guess of $I_i^{\pm}(x)$ at the left most section x = 0 and *i* denotes the mode. The population inversion is obtained by solving Eq. (3.29) given dn/dt = 0 at steady state with Newton root finding. $k = h*f(n(0), I_i(0))$ is calculated and then the midpoint of the next section $I_i(h/2) = I_i(0) + k/2$ is calculated. At this middle step, we get the inversion population n(x) again to be more accurate, and then intensity of next section $I_i(h) = I_i(0) + h*f(n(h/2), I_i(0) + k/2)$ is calculated. The same steps are repeated until the optical power of the last section is obtained.

The boundary condition must be satisfied at the front facet, which are written as $I_i^-(64*h) = R_{eff}^{coh}(\nu)\, I_i^+(64*h)$ and $I_i^+(64*h) = I_i^-(64*h) / R_{eff}^{coh}(\nu)$. The key point here we have to mention is that the incoherent part $(1-\gamma)$ of feedback light from the FBG external cavity should be added in the form of spontaneous emission at the right most section n = 64. Equation (3.12) is applied here. This incoherent feedback light together with the optical waves in the cavity will experience amplification on the way traveling back to the back facet. After applying boundary condition at the back facet, the criterion of χ^2 was used to determine whether steady state of the diode laser has been obtained or not. χ^2 is defined as $\chi^2 = \Sigma_i[(I_{i,m}-I_{i,m-1})^2/I_{i,m}{}^2]^2$. If not, iteration will continue until the precision of χ^2 is satisfied (10^{-4} in my calculation).

The parameters used for calculation of traveling wave method are listed in table 3.3

Table 3.3 Values of laser parameters for calculation

A	1×10^{8} (/s)
B	5×10^{-10} (cm^3/s)
C	1×10^{-34} (cm^6/s)
β	3.2×10^{-4}
η	0.5
L (Laser cavity length)	1000 μm
$g_{i,max}$	2.5×10^{-16}(cm^2)
R_b	0.93
R_f	0.04
N_{sect}	64
N_{modes}	51

These parameters are adjusted to fit the L-I curve which is the output power versus injected current at the back facet of the real 980-nm pump laser for measurement when there is no FBG feedback. Figure 3.9 is the L-I curve with 51 modes added which is consistent with the true case of the laser with FBG. The threshold current of the solitary laser is 23.9 mA.

When the FBG is included, a reduced threshold current and increased quantum efficiency will reshape the L-I curve. The quantum efficiency will depend on the coherence parameter. By varying the coherence parameter γ from $\gamma = 1$ (coherent interaction) to $\gamma = 0$ (incoherent interaction), the quantum efficiency and the slope of the L-I curve will change correspondingly. Figure 3.10 (a~e) shows the computer generated plots of the difference in the total output power as a function of the pumping rate under feedback and no feedback with varying γ values. The relationship of photon number to the optical output power was applied as:

$$P_m = I_m(1 - R_b)wd\frac{hc}{\lambda} \tag{3.35}$$

The relationship between the pumping rate N and the injection current is given by:

$$J = pump * qdwL$$

where w, d are the width and depth of the active region of the laser.

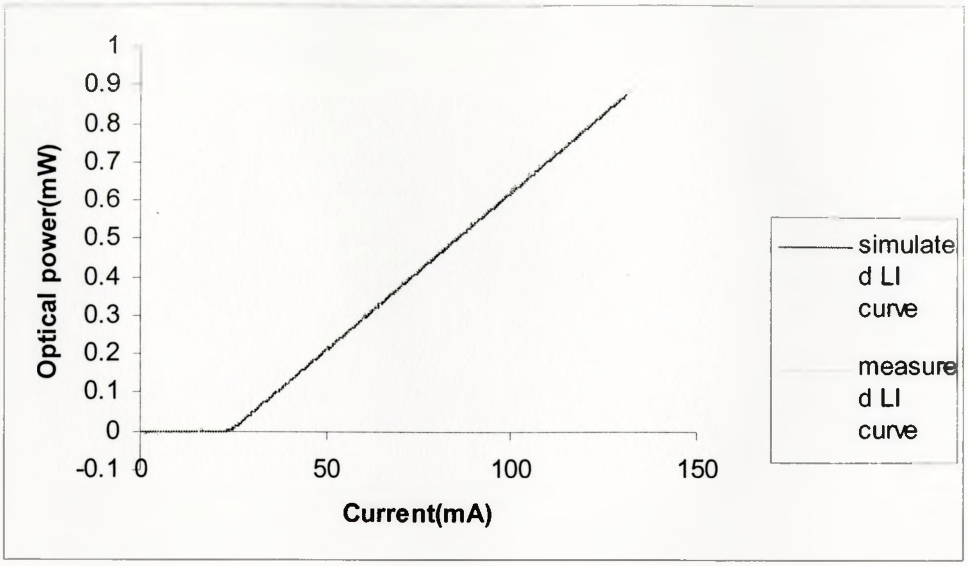

Fig.3.9 L-I curve of back facet output power of the solitary laser

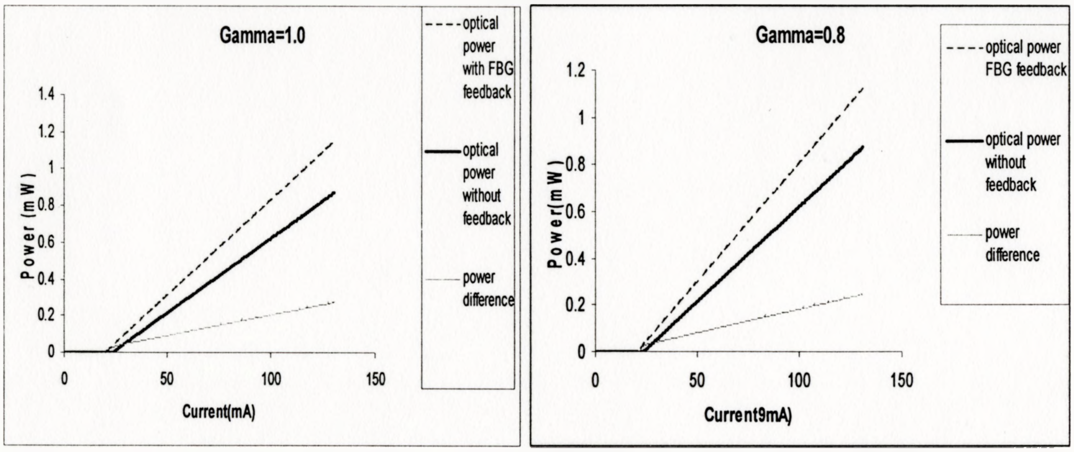

(a) (b)

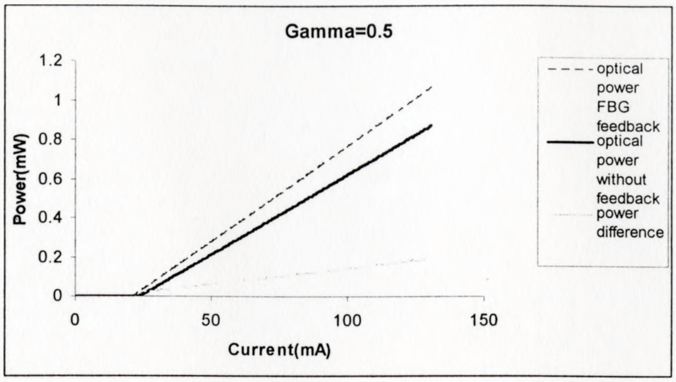

(c)

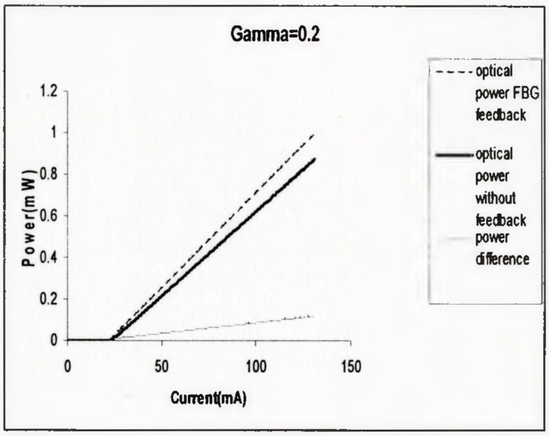

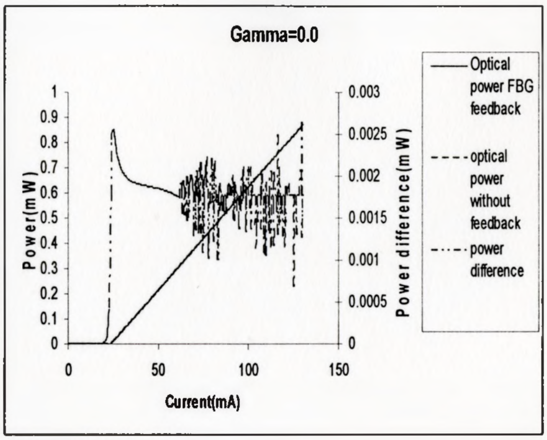

(d) (e)

Fig. 3.10 Computer-generated power difference versus injected current under different coherence parameter γ = 1.0, 0.8, 0.5, 0.2, and 0.0 for (a ~ e) respectively.

From Fig. (3.10) it is obvious that the different amount of feedback light which is assumed to interact coherently with the field in the laser cavity causes drastically different effects on the output power of the laser. The higher is the coherence parameter, the higher the slope of the power difference curve. All the plots are based on the output power at the back facet of the laser diode. The relationship between the output powers of each end of the laser is governed by [42]:

$$\frac{P_b}{P_f} = \frac{(1-R_b)\sqrt{R_f}}{(1-R_f)\sqrt{R_b}} \tag{3.36}$$

Figure 3.10 indicated that the coherence parameter γ can be figured out by measuring the power difference curve, and fitting it to the simulation results. To get different coherence parameter, experiment parameters such as the length of the external cavity (fiber length from the front facet to the FBG) and the amount of feedback (changed by the ND filter) will be changed. Experimental measurements and the fitting results will be introduced in next chapter.

3.5 Gain spectrum

Wavelength spectra of gain g_i appeared in Eq. (3.31~3.33) can be obtained by measuring the depth of modulation introduced into the spontaneous emission spectrum by the Fabry-Perot resonance. Max/min method was first introduced [43] by Hakki and Paoli. A renovated method named sum/min approach was introduced by Dr. Cassidy [41] to improve the accuracy of the gain measurement. The latter may reduce the remaining effects of the response function of the spectrometer used in the measurement. According to sum/min method, the mth mode single pass gain G_m ($G_m = \exp(g_m L)$) is:

$$G_m = \frac{1}{\sqrt{R_f R_b}}\left(\frac{p-1}{p+1}\right) \tag{3.37}$$

where $p = \frac{c}{2l} p'$, and p' is the ratio of the mth mode sum to the mth minimum which are obtained by the FP modulation introduced into the spontaneous emission spectrum. Schematic of sum/min method is shown in Fig. (3.11)

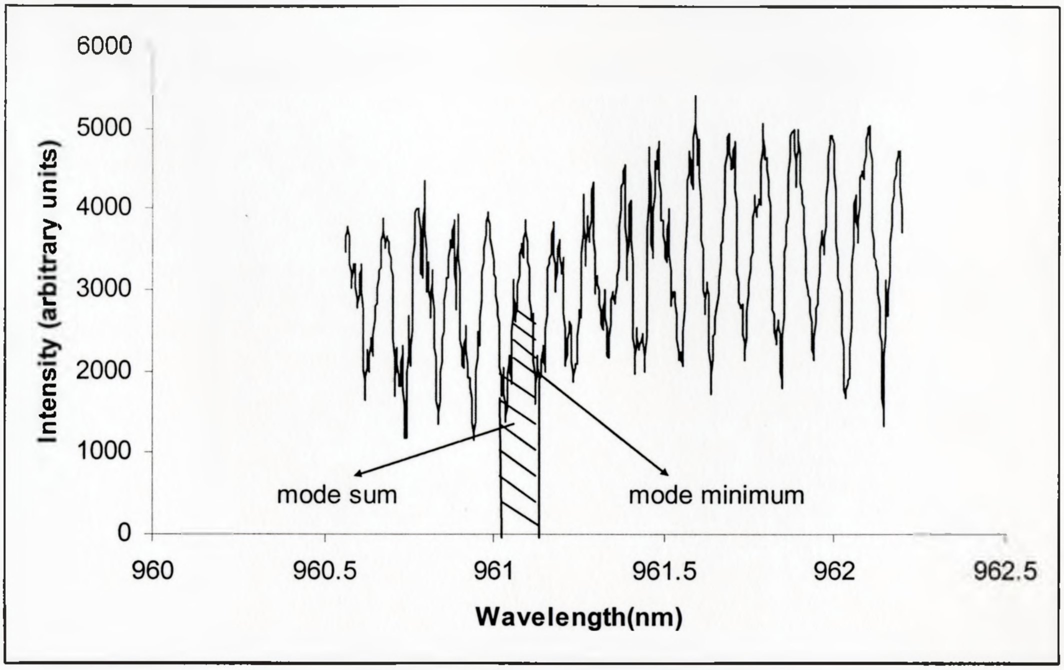

Fig. 3.11 Schematic of sum/min method of acquisition of gain spectra.

The experimental gain profile was determined for 980-nm pump laser at bias current of 24 mA and the smoothed data is plotted in Fig. 3.12 by normalizing maximum differential gain to 1.

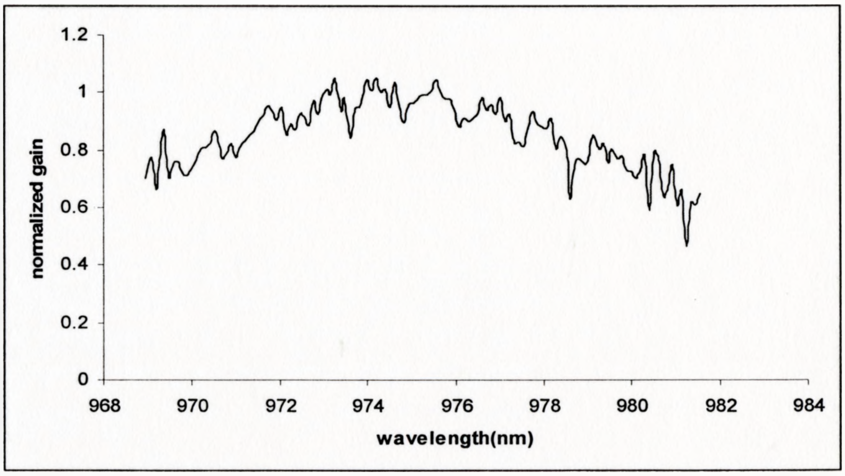

Fig.3.12 Gain spectrum (normalized to 1) under injection current I = 24 mA

In the simulation of 980-nm pump laser, the analytical form of gain spectrum is needed. Thus the nonlinear, least square fit to arbitrary curve was applied. The gain vs. wavelength formula is written as:

$$g_i(\lambda) = a + b\lambda + c\lambda^2 + d\lambda^3 + e\lambda^4 \qquad (3.38)$$

The fitting result is shown in Fig. (3.13) using a = 0.5971, b = -0.08163, c = 0.001085, d = 0.0009921, e = 0.00003659, λ in Eq. (3.38) is the value which is the actual wavelength minus 980 nm for the fitting convenience.

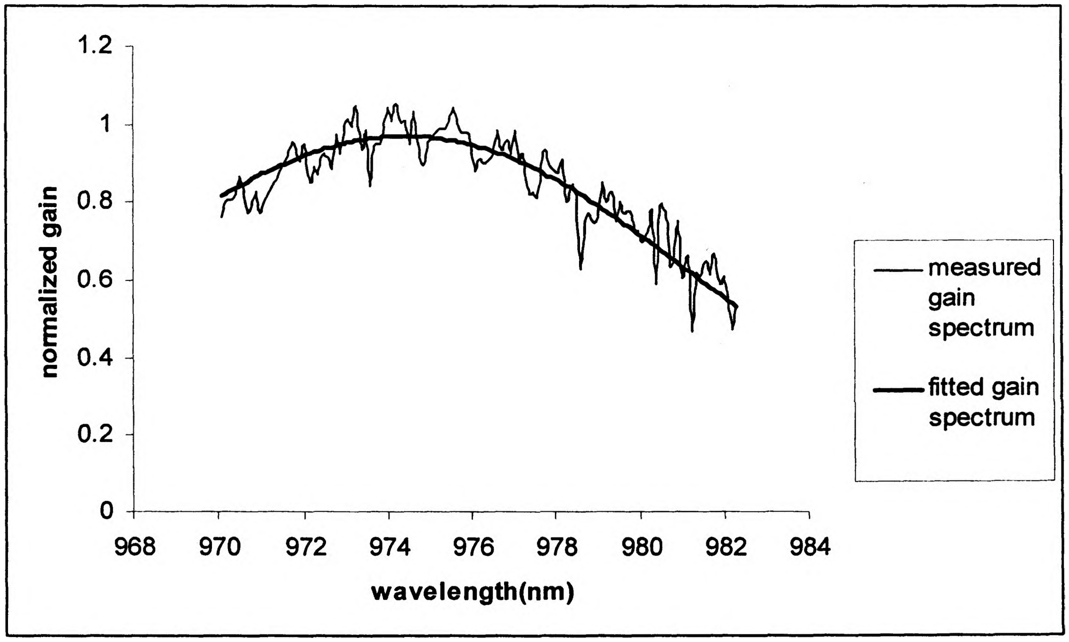

Fig.3.13 The fitting result of gain spectrum under current of I = 24 mA

The effect of nonlinear gain of the high power 980-nm pump laser has to be taken into account. The symmetric model of nonlinear gain caused by spectral-hole-burning mechanism was adopted [44]:

$$g_i = g_i(\lambda_i) = \frac{g_0(\lambda_i)}{1 + \frac{1}{\pi w} \sum_{m=1}^{N_{modes}} \frac{d \times (I_m^+ + I_m^-)}{1 + (\frac{\lambda_i - \lambda_m}{w})^2}} \tag{3.39}$$

where w and d are the width and the depth of the Lorentzian hole especially. In the model, a gain-suppression term linear with the mode power is added to the expression for the gain g_i for the ith mode. The gain-suppression term allows for the gain at mode i to be affected by the holes in each mode. $w = 0.5$ nm and $d = 0.01$ were applied in our simulation.

3.6 Summary

Modeling of partial coherent interaction of feedback light with the light in the laser cavity is introduced in this chapter. Applying traveling wave model with the effective reflectivity method, the coherent part of feedback light has obviously different effect in the laser cavity with the incoherent part. This would be shown in the power difference versus injection current curve. The gain spectrum was acquired with the sum/min method from the emission spectra of the laser. Symmetric nonlinear gain, which is caused mainly by spectral hole burning, was taken into account for the high power pump laser.

CHAPTER 4 EXPERIMENTS AND RESULTS

4.1 Introduction

This chapter describes the experimental techniques developed for measuring the power difference for 980-nm pump laser when it is under feedback and no feedback. A description of the optical apparatus in the context of power difference measurement is given in section 4.2. The coherence parameter may be obtained by fitting the simulation results to the measured power difference curve. Three elements including mirror, blazed grating and FBG were applied for the coherence parameter acquisition. These are introduced in section 4.3. Analysis and discussion are given in section 4.4.

4.2 Description of Apparatus

Figure 4.1 is a schematic of the optical and electronic apparatus.

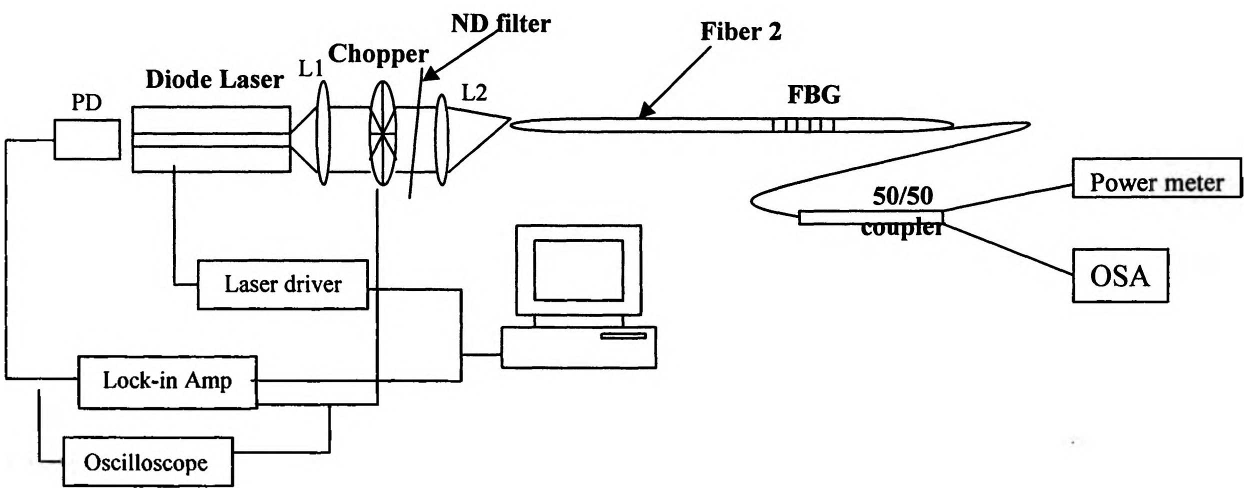

Fig.4.1 Schematic of power difference measurement

The laser under test was a fiber pigtailed InGaAs/GaAs semiconductor Fabry-Perot laser supplied by Alfalight Incorporation. Its threshold current at room temperature is

23.9 mA with differential efficiency 0.36 mW/mA at the front facet which was AR coated to a reflectivity of 0.04. Applying Eq. (3.36), we achieved differential efficiency of 0.008 mW/mA at the back facet with $R_b = 0.93$. The kink power of this laser is as high as 120 mW without FBG stabilization. The spectra of this solitary 980-nm pump laser are shown in Fig. 4.2 under room temperature at currents of I = 24, 84, 168 and 204 mA. The central wavelengths shift red with the increasing injection current as well-known reason of gain peak shifting.

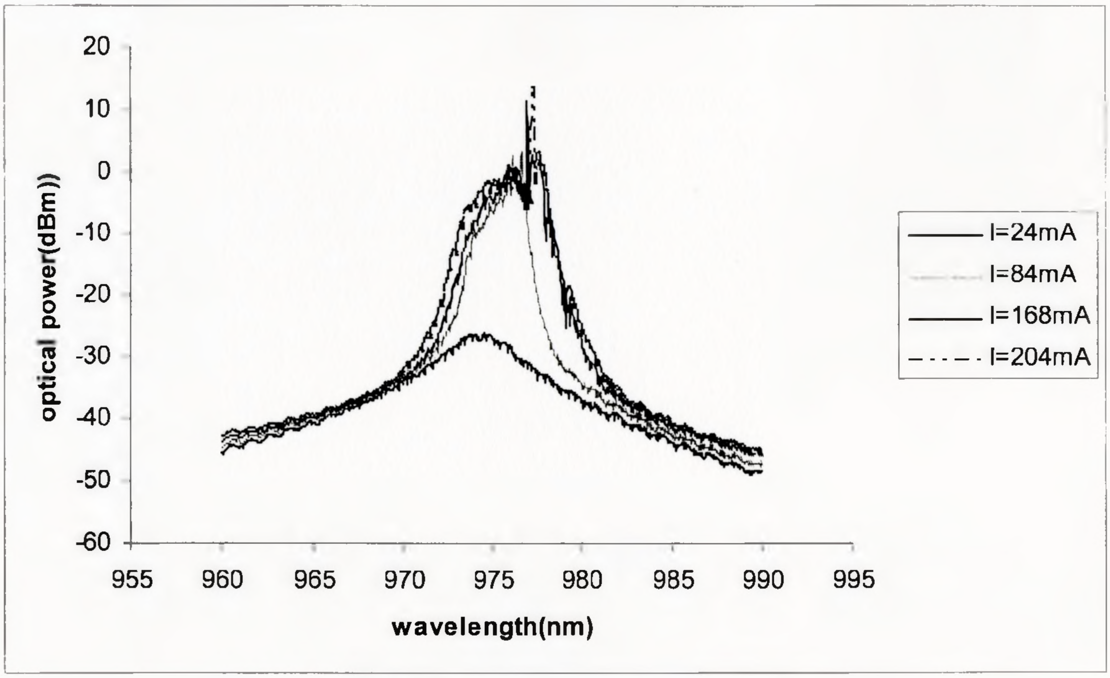

Fig 4.2 Spectra of 980-nm solitary laser

The fiber Bragg grating was purchased from Bragg Photonics Corp., with central wavelength of 977.80 nm and maximum reflectivity of 4.14%. Its full width half maximum (FWHM) of bandwidth is 1.47 nm.

The light from the laser fiber tail was collimated by a fiber collimator (Thorlabs F220FC-C). There was a break before the laser light was coupled back into a second fiber which had a FBG for feedback. An objective lens and a fine positioner which held the end of the second fiber were used as the coupler. The positioner has 3 axes translational and 3 rotational adjustment to adjust the position and the angle of the fiber end. A mechanical chopper was placed in the feedback arm. The output from the back facet of the laser was detected by a photo detector (PD) and processed with a lock-in amplifier referenced to the chopper frequency. The lock-in amplifier phase settings were chosen to maximize the signal and resulted in a significant improvement in signal-to-noise ratio (SNR). The chopper frequency was set to be 1kHz (T = 1ms) and the external cavity photon lifetime is about ($L_{ext}/c = 2/(3*10^8/s)$) one nanosecond. Therefore the laser was able to get steady state within one chopper period. The steady state theory is applicable to this measurement set-up. What the lock-in amplifier read is the power difference at back facet when the laser is under feedback (chopper 1) and no feedback (chopper 0). ND filters were used to adjust the amount of feedback in the feedback arm.

All the feedback was supposed to be only from FBG. All other feedback caused by components in the experiment set-up is called unwanted feedback. To minimize the unwanted feedback, the fiber collimator (Thorlabs F220FC-C) was AR coated. The ND filter and the chopper were placed tilted to avoid reflecting back to the laser cavity. The convex surface of the objective lens L2 faced the front facet of the laser cavity. The fiber end was angle cleaved to 8^0 to avoid fiber tip reflectivity. With these arrangements, dominant feedback was from the fiber grating. The numerical aperture (NA) of the objective lens L2 was chosen to be as close as NA of single mode fiber HI1060 which is 0.14 to improve the coupling efficiency. The maximum coupling efficiency was obtained when the angle cleaved fiber end was placed at the focal point of the objective lens, and was aligned very well to the laser beam. The maximum coupling efficiency acquired from this apparatus was about 60%. A 50/50 (2×2) single mode fiber coupler was used to monitor the output. One arm of the fiber coupler was used as input, one output arm was connected to the power meter (Newport 1830C) and the other output arm to the optical spectrum analyzer (OSA). The free arm of this coupler at the input side was put in a matching index of glycerine to avoid reflection.

The spectra of 4% FBG stabilized 980-nm pump laser under various injection current are shown in Fig. 4.3. The feedback provided by the grating locks the laser to the wavelength defined by the FBG and it will not shift with the increasing current as shown in Fig. 4.2.

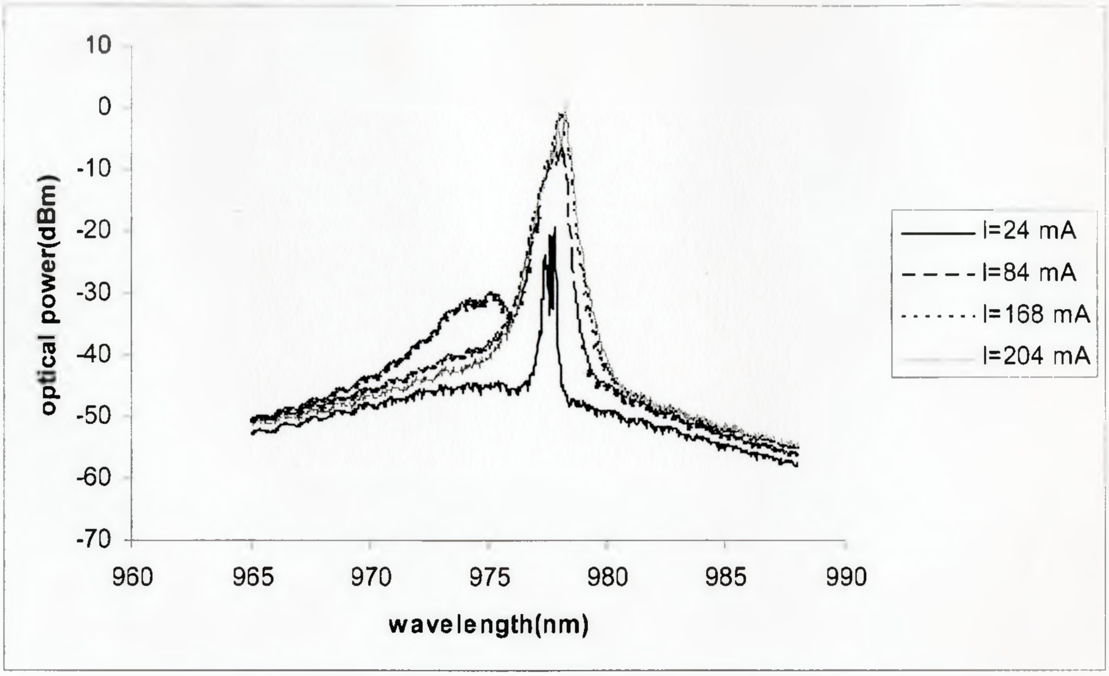

Fig.4.3 4% FBG stabilized 980-nm pump laser spectra

4.2.1 Amount of feedback

To inspect the amount of feedback under this circumstance, we used the criteria of Tkach [14] by defining:

$$\kappa = 10\log_{10}\frac{P_e}{P_f} \qquad (4.1)$$

where P_f is the optical power at the front facet, P_e is the power fed back into the laser cavity. In this case with 4% FBG, and 50% coupling efficiency, κ = -20 dB. This accorded with the working regime of "coherence collapse".

4.2.2 Polarization effect

The light emitted by the laser is linearly polarized along the transverse-electric direction of the waveguide (TE polarization). However, the fiber commonly used is non-polarization maintaining fiber, thus the change of polarization should be taken into account. The effects of polarization change in feedback provided by fiber Bragg gratings on stabilized 980-nm pump laser were investigated in papers [45], [48]. Because the light reflected from the FBG into the laser cavity can undergo a change of polarization, it will result in loss of effective feedback, as only TE-polarized light contributes effectively to the locking. The effective reflectivity of the grating is given by $R = R_{rel}R_{fbg}$, where R_{rel} is relative effective reflectivity which is related to the bending angle of the fiber coil. We could observe the polarization effect by bending the fiber 2. To minimize the effect of polarization, we kept the fiber coil parallel to the TE direction, therefore $R_{rel} \approx 1$ in our experiment.

4.3 Measurements and fitting results

According to former researches [14] [15], at "coherence collapse" regime, the spectral details which are shown as external cavity peaks in emission line shape at lower feedback level disappear until finally one single dramatically broadened line results with a width of the order of 25 GHz. The spectral features of the laser light have become independent of the external cavity length. The coherence length of the laser light, therefore, will clamp to about 10 mm with the level of high feedback. Suppose that the coherence length will not change much in our measurement by keeping it in regime IV, we measured the coherence parameter γ (thus the fraction of feedback light which is interacting coherently with the field in the laser cavity) by changing the length of the external cavity. That is done by moving the feedback elements (FBG, mirror, blazed grating) closer or further away from the front facet, as shown in Fig. 4.1. In our expectation, the shorter is the external cavity, the higher the coherence parameter γ should be ($0 < \gamma < 1$). The other factor affecting the shape of the power difference curve is the amount of feedback which can be altered by the value of R_{ext}, and the ND filter placed in the feedback arm. Therefore two series of measurement were done with this experimental set-up. One was for relationship between the coherence parameter and the external cavity length; these results are given in Section 4.3.1. The other was for the relationship between the coherence parameter and the amount of feedback which can be changed by ND filter in the feedback arm. This is given in Section 4.3.2.

4.3.1 γ versus length of external cavity

4.3.1.1 FBG feedback

With the abovementioned set-up and fiber Bragg grating of peak reflectivity 4%, we changed the length of the external cavity by cutting and fusing the fiber 2. In this process, the coupling efficiency was monitored by the power meter to keep it stable. In the whole process of measurement, the laser was held working at a temperature of 24^0C. The laser driver and the lock-in amplifier were remotely controlled by the computer with A/D and D/A conversion channels.

Figure 4.4 shows the power difference curves measured with this set-up. Five lengths of FBG external cavity were used: 60 cm, 150 cm, 240 cm, 360 cm, and 450 cm separately. The humps and bumps on the power difference curve are a reproducible feature of the difference, and are result of the gain peak and lasing modes position changing with the injection current. The LI curve at the back facet is shown for reference in these figures. The maximum output power at back facet corresponds to a maximum output power of 58 mW at the front facet. 60 cm (30 cm for the fiber tail, 10 cm for the break and 20 cm for the fiber 2) is the closest distance we can get with the limitation of the fiber splicer we worked with. From Fig. 4.4 we can see that the shapes of the power difference curve are different with different external cavity length, and the trend is as what we expected -- longer external cavity has smaller slope of the power difference curve. The different slope may related to the different coherence parameter as predicted in chapter 3 (Fig. 3.11 (a ~ e)).

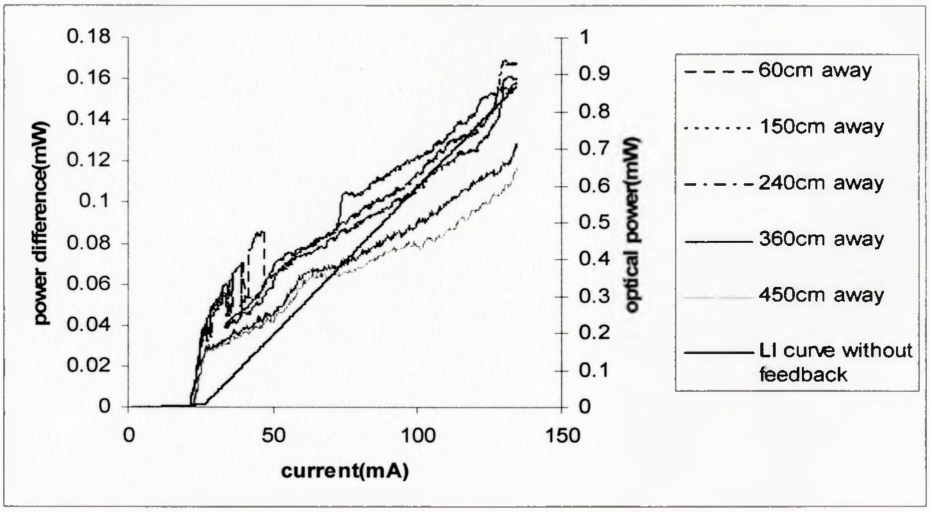

Fig.4.4 FBG feedback, measured power difference curve with different distance from FBG to the front facet

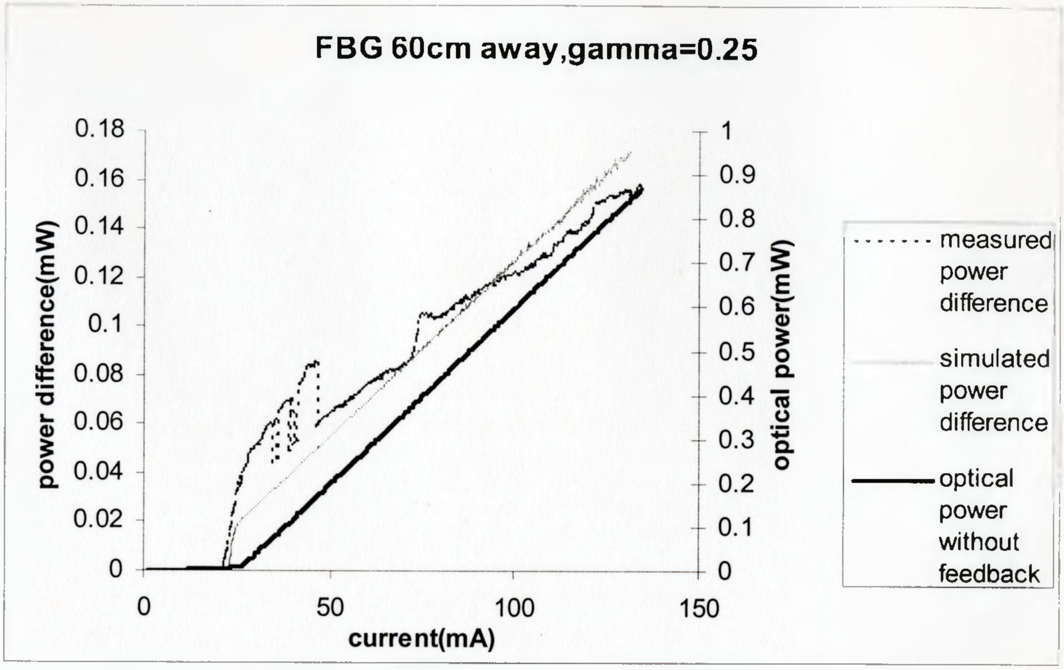

FBG 60cm away,gamma=0.25
power difference(mW)
0.18
0.16
0.14
0.12
0.1
0.08
0.06
0.04
0.02
0
optical power(mW)
1
0.9
0.8
0.7
0.6
0.5
0.4
0.3
0.2
0.1
0
0
50
100
150
current(mA)
measured power difference
simulated power difference
optical power without feedback

(a)

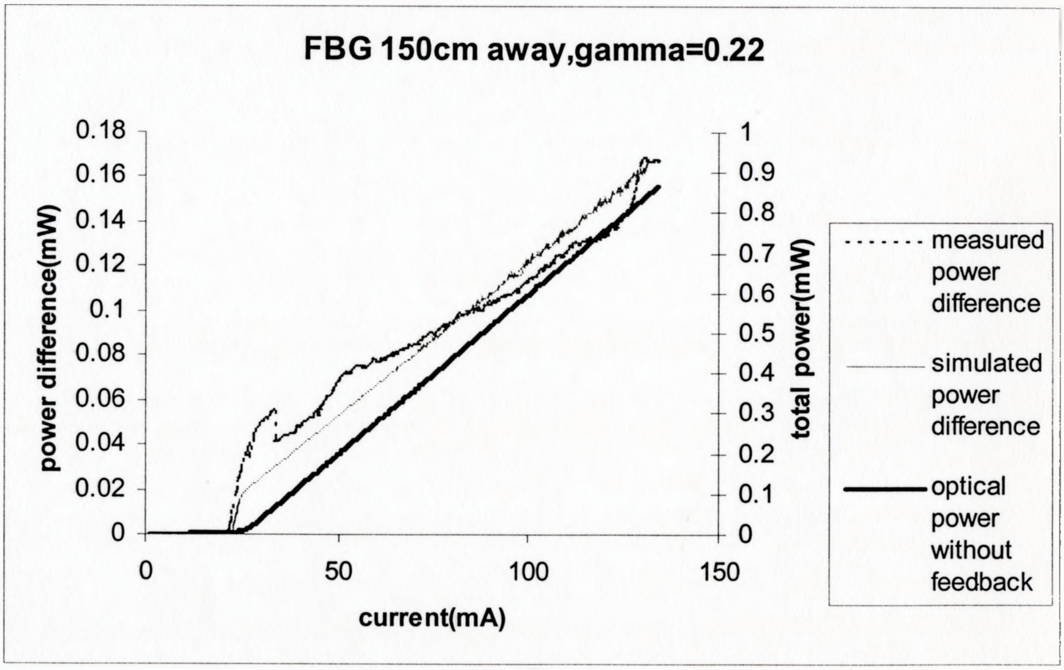

FBG 150cm away,gamma=0.22
power difference(mW)
0.18
0.16
0.14
0.12
0.1
0.08
0.06
0.04
0.02
0
total power(mW)
1
0.9
0.8
0.7
0.6
0.5
0.4
0.3
0.2
0.1
0
0
50
100
150
current(mA)
measured power difference
simulated power difference
optical power without feedback

(b)

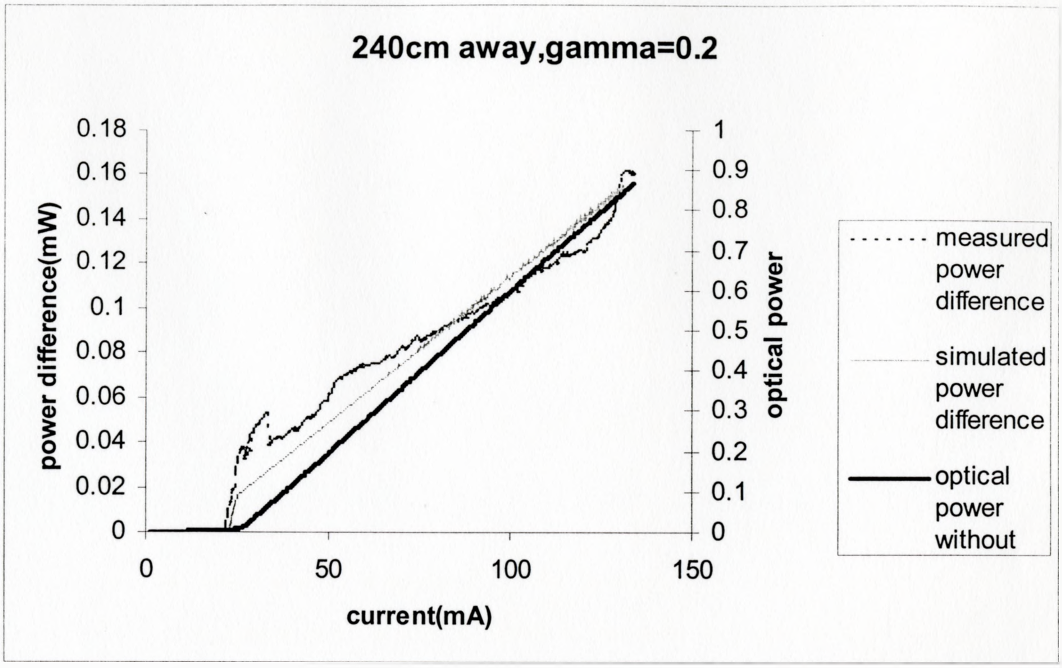
240cm away,gamma=0.2
0.18
0.16
0.14
0.12
0.1
0.08
0.06
0.04
0.02
0
power difference(mW)
1
0.9
0.8
0.7
0.6
0.5
0.4
0.3
0.2
0.1
0
optical power
0
50
100
150
current(mA)
measured power difference
simulated power difference
optical power without

(c)

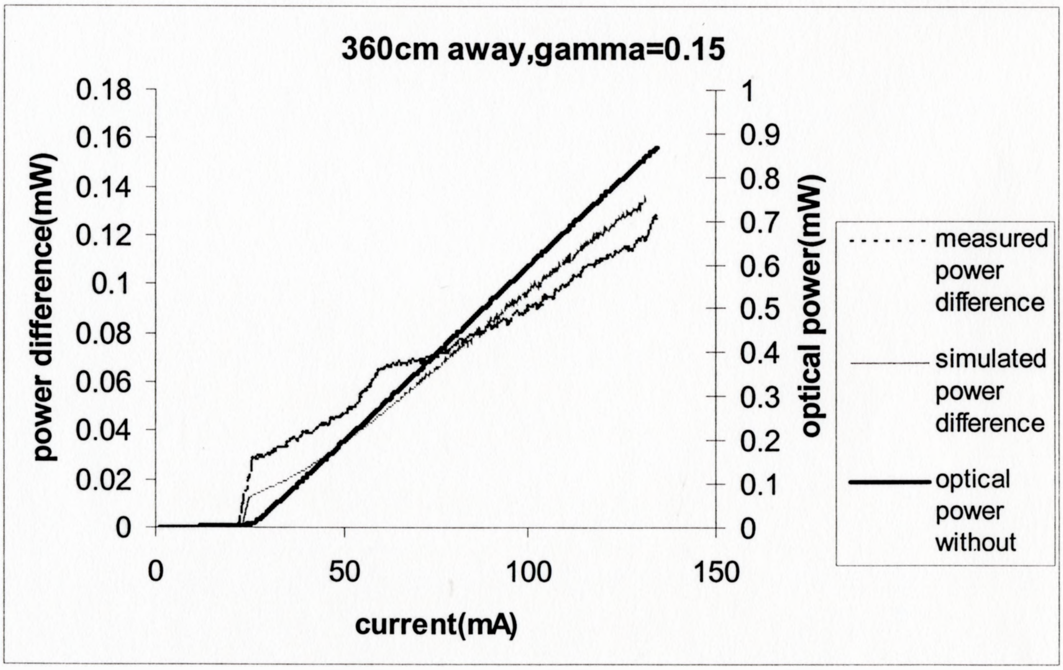
360cm away,gamma=0.15
0.18
0.16
0.14
0.12
0.1
0.08
0.06
0.04
0.02
0
power difference(mW)
1
0.9
0.8
0.7
0.6
0.5
0.4
0.3
0.2
0.1
0
optical power(mW)
0
50
100
150
current(mA)
measured power difference
simulated power difference
optical power without

(d)

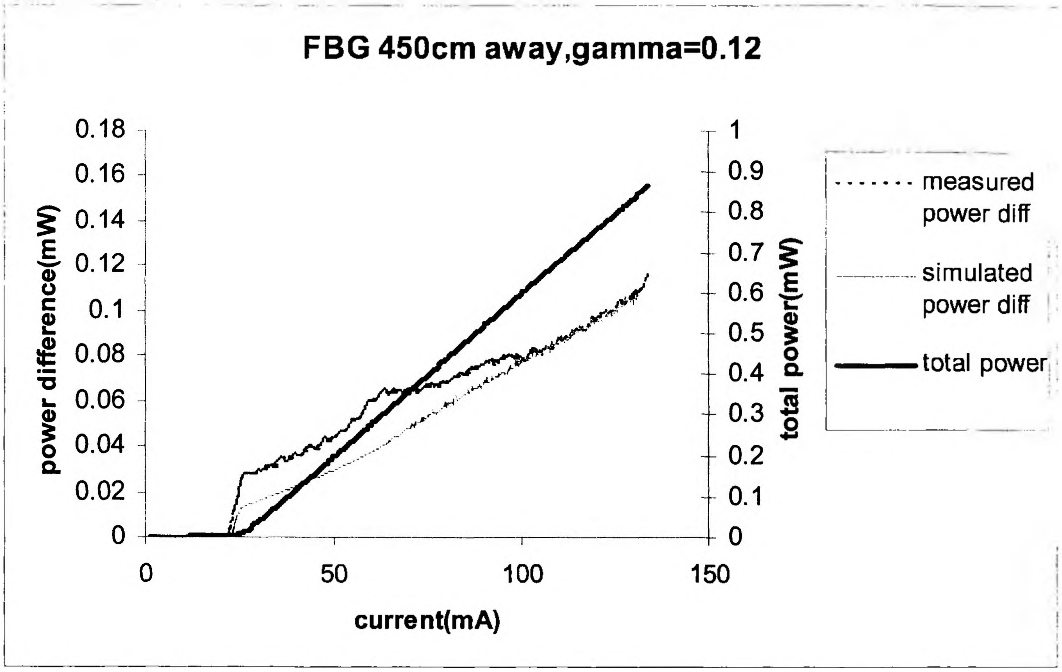

(e)

Fig.4.5 Fitting results of measurement results to simulated results by changing coherence parameter γ. (a) $\gamma = 0.25$, $L_{ext} = 60$ cm.(b) $\gamma = 0.22$, $L_{ext} = 150$ cm. (c) $\gamma = 0.20$, $L_{ext} = 240$ cm. (d) $\gamma = 0.15$, $L_{ext} = 360$ cm.(e) $\gamma = 0.12$, $L_{ext} = 450$ cm

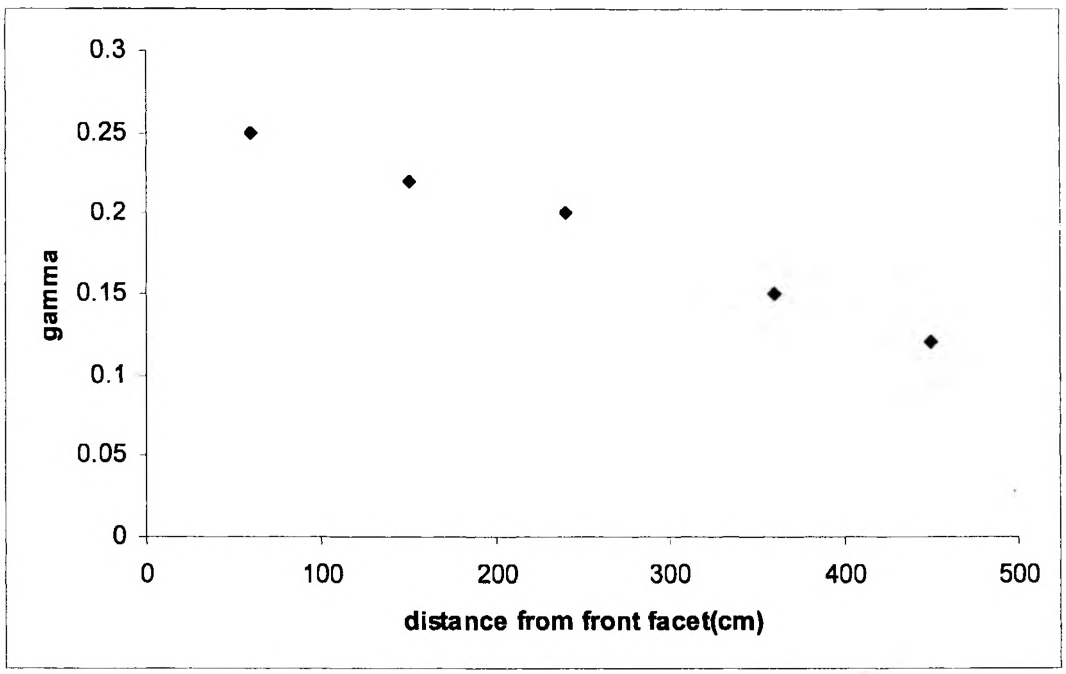

Fig. 4.6 Relationship between the coherence parameter and the distance of FBG from the front facet based on fitting results

Fitting procedures were done by choosing simulated results of power difference curve with various value of γ to fit the measurement results. Figure 4.5 (a ~ e) show the fitting results for each measurement with different coherence parameters of $\gamma = 0.25, 0.22, 0.20, 0.15$ and 0.12. In the fitting procedure, the slope rather than the fit at each point of the curve was considered. The relation between the coherence parameter and the length of external cavity is shown in Fig. 4.6 for the 5 lengths of Fig. 4.5. From these results, we can see that for the long external cavity which is working in the so-called "coherence collapse" regime, there is actually a small part of the feedback light interacting coherently with the field established in the laser cavity. This fraction might be between 10% and 25% depending on the length of the external cavity. It may increase further to 100% when the laser is working with the short external cavity regime [46]. On the other hand, it may decrease to very small for an extreme long distance of feedback. To confirm this point, we made a measurement with FBG 25 meters away from the front facet and the fitting result is shown in Fig. 4.7 (a). It is shown that the coherent fraction of interaction reduces to 0.07 when FBG is far enough. The uprising after 100 mA means more coherent interaction occurring for high power operation. To see that coherence parameter will never be smaller than 0, we made a measurement with much longer fiber which put the FBG 25, 50, 75 meters away. The results are shown in Fig. 4.7 (b). We can see that the slope of power difference curve would not go further lower after we get very small part of incoherent interaction for long enough external cavity. Therefore we conclude that the coherence parameter may saturate to a small number for long external cavity.

The other feature we may see from the power difference curve is that its slope may change with the injection current. So the coherence parameter is not constant for any current, we may say that it is function of current, $\gamma = \gamma (I)$. This feature also shows in the following measurements.

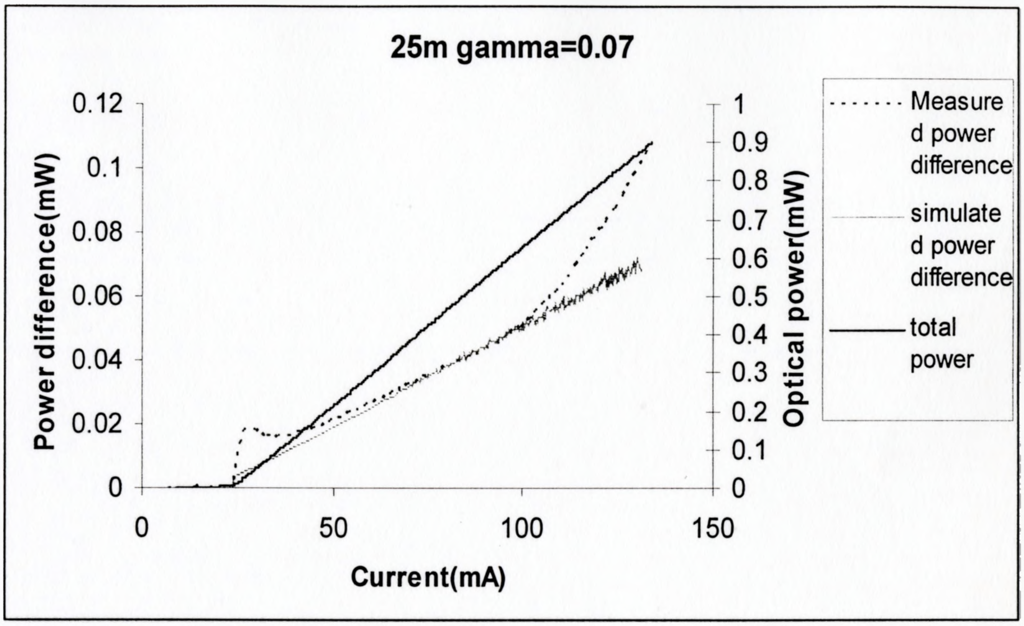

(a)

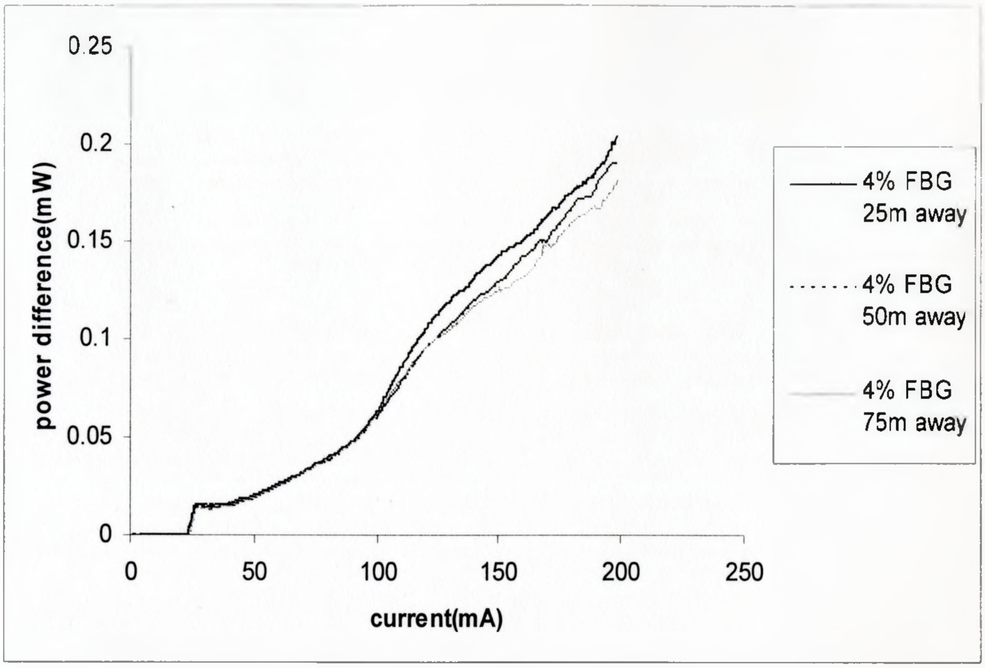

(b)

Fig.4.7 (a) FBG 25 meters away fit to $\gamma = 0.07$. (b) Comparison of power difference curve of 25,50,75 meters away.

From the above measurement and fitting results, we can conclude that in the normal case of an FBG stabilized 980-nm pump laser with 2-meter length of external cavity, the coherence parameter is about 0.20 ~ 0.22 according to our measurement.

4.3.1.2 Mirror feedback

To compare and confirm the results, we also made measurements with mirror and blazed grating feedback with free space external cavity. The results with mirror feedback are given in this section in Fig. 4.8. Similar simulation procedures as introduced in chapter 3 were done with mirror replacing the fiber Bragg grating for feedback. For 65 cm length of external cavity, γ is fit to be 0.1, and for one meter external cavity, γ is about 0.02. The coherence parameter is much smaller in the case of mirror, because mirror has no wavelength dependence reflectivity.

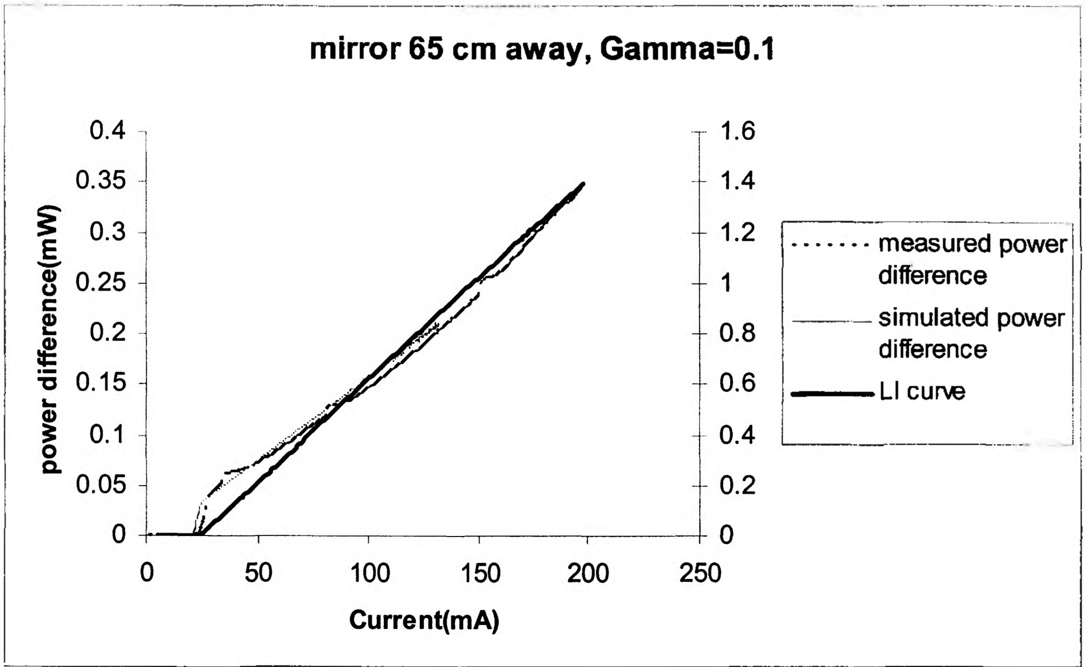

(a)

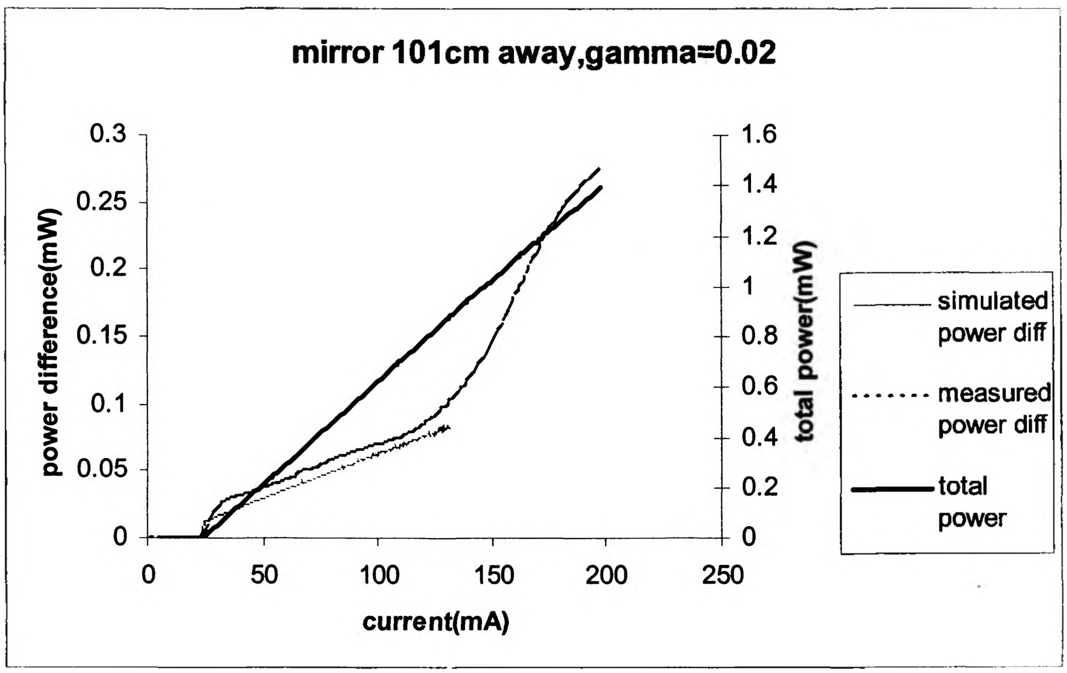

(b)

Fig.4.8 Measurements with mirror feedback. (a) L_{ext} = 65 cm, γ = 0.1. (b) L_{ext} = 101 cm, γ = 0.02

4.3.1.3 Blazed grating feedback

Littrow configuration was constructed for the grating external cavity feedback to replace the FBG in this measurement. The blazed grating was held in a gimbal mount and placed with grating lines perpendicular to the diode laser junction plane for TE polarization. The grating used in this work was a 600 line mm^{-1}(blazed angle 22.02^0 at 1.25 μm). The first order diffracted beam was reflected collinear with the incident beam and re-imaged onto the end of the fiber tail. Although the light is reflected in a band of frequencies, only one diode laser internal mode will be selected at a given orientation of the grating, because of the small aperture of the fiber core [19], [47]. Simulations were done for the grating feedback to fit the measurement results as shown in Fig. 4.9. For 69 cm length of external cavity, γ is fit to be 0.5, and for one meter external cavity, γ is about 0.3. Coherence parameter is much higher because of the wavelength selectivity (single mode feedback) of the grating.

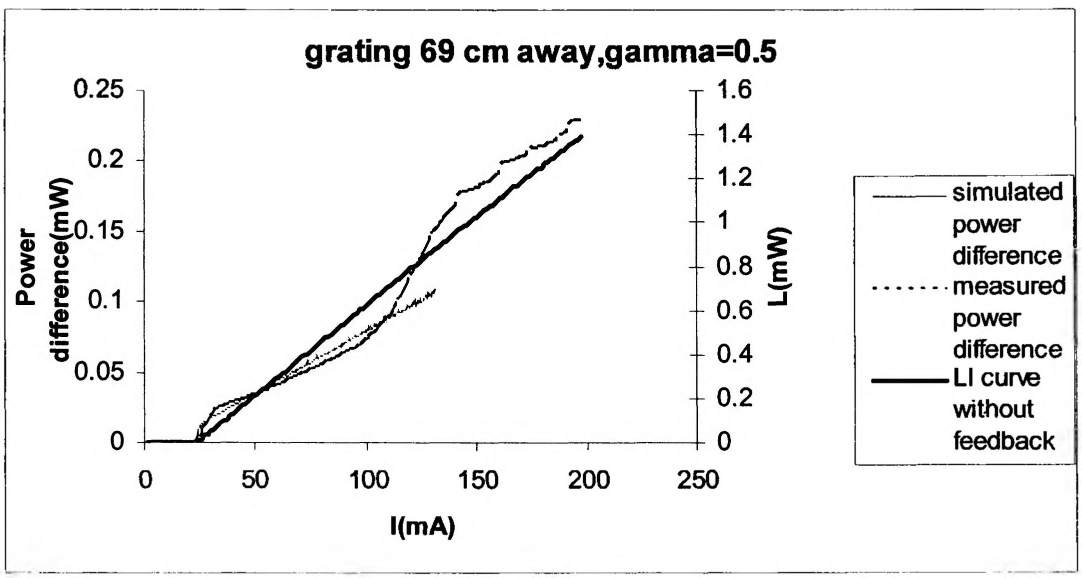

(a)

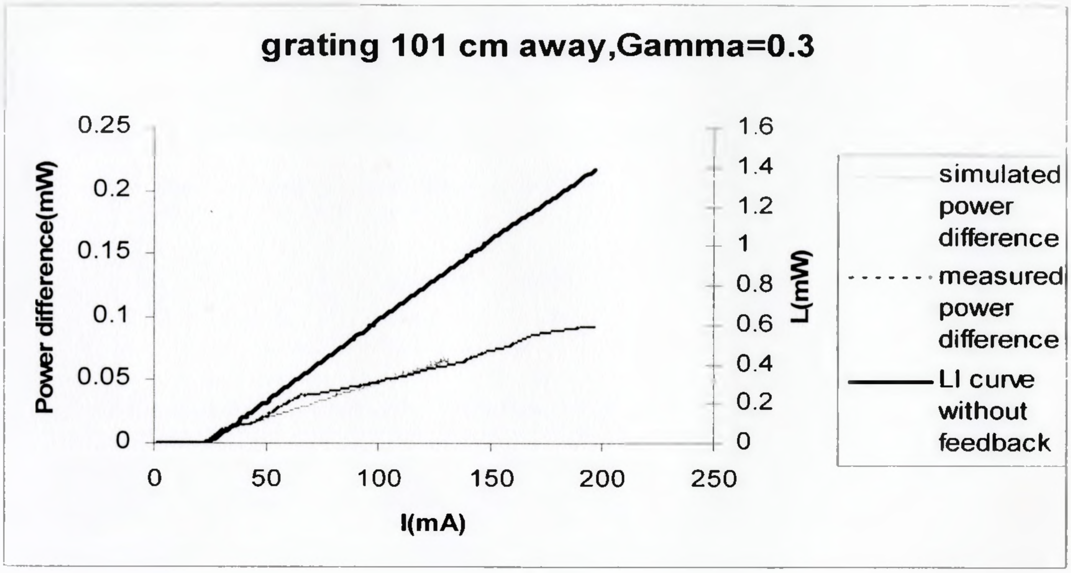

(b)

Fig. 4.9 Measurement with grating feedback. (a) $L_{ext} = 69$ cm, $\gamma = 0.5$. (b) $L_{ext} = 101$ cm, $\gamma = 0.3$

Comparing the above three cases of feedback, we can conclude that the coherence parameter depends on the wavelength selectivity property of the feedback element. With the same external cavity length, γ is the highest for the blazed grating feedback and is the lowest for the mirror feedback. For the FBG with full width half maximum (FWHM) 1.47 nm, γ lies between the other two cases. Therefore, we expect that by changing the FWHM of the FBG, we can change the fraction of feedback light which is interacting coherently with the field in the laser cavity.

4.3.2 γ versus amount of feedback

The relationship of amount of feedback and the coherence collapse was probed with a FBG which has a high peak reflectivity of 73%. The FBG was fused 200 cm away from the front facet and would not change in the process of measurement. ND filters were placed tilted behind the chopper to avoid unwanted feedback as shown in Fig. 4.1. The three ND filters I used in this measurement were ND = 0.1, 0.2 and 0.3 respectively.

Their transmissions are given Table 4.1. Note that the optical density is related to the transmission T by ND = $-\log_{10}T$.

Table 4.1 List of neutral density filters and their transmissions

transmission(T)	Optical Density(ND)
79.43%	0.1
63.10%	0.2
50.12%	0.3

The key issue in this measurement to choose ND filters is that we have to keep the system working in the region in which the amount of feedback is between -40 dB and -10 dB. For the coupling efficiency about 35% in my experiment set-up, they are -11 dB, -13.3 dB and -15.3 dB for ND = 0.1, 0.2 and 0.3.

In the simulation program, the coefficient of η has to be changed to adjust the amount of feedback. That is why the slope of power difference curve is lower for higher ND number for the same coherence parameter. The fitting results are shown in Fig. 4.10. From the fitting results we can see that the coherence parameter would not change much if we change the amount of feedback while keep the length of external cavity constant. The coherent part of feedback stays all around 0.1 for the distance 200 cm. This is consistent with the former observation that the broadened linewidth in coherence collapse state would not change much in this stage [14]. However from the comparison of the four fitting curves, we can see the slope of the measured power difference curve turns a little bit higher than the simulation result when ND is smaller. Therefore the coherence parameter becomes a little bit larger as the raising of the feedback level in this regime. This trend may grow until it goes to the regime V of feedback, in which the linewidth get extremely narrowed because the laser ideally operates in a long cavity with a short active region and the feedback dominates the field in the diode laser.

One feature we need to mention is that by high peak reflectivity FBG, we observe an obvious kink. And the slopes of the power difference curve before and after the kink are a little bit different. This means that the coherence parameter may be different before and after the kink power. The trend is that the coherent interaction after the kink point is higher than it is before the kink point. This doesn't show at low peak reflectivity and may be taken as the effect of high reflectivity FBG.

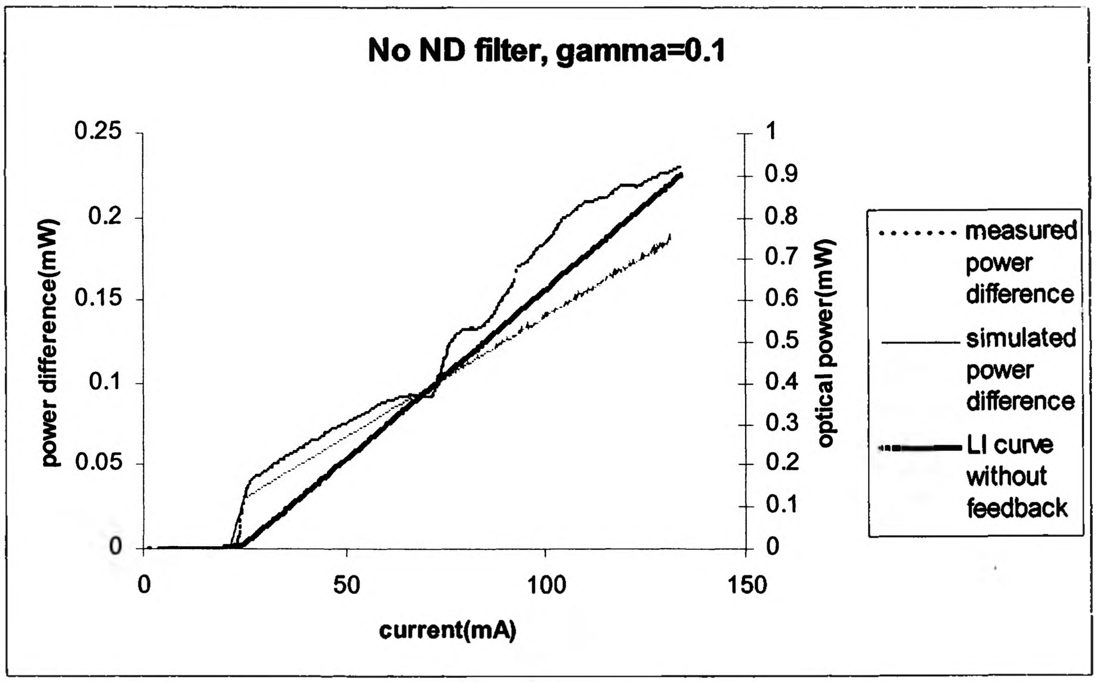

(a)

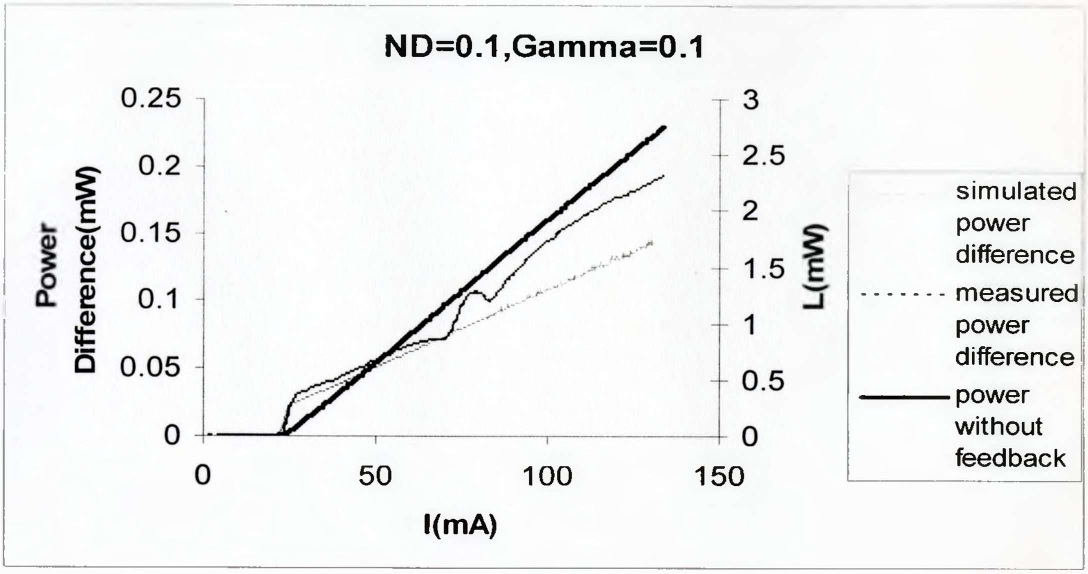
ND=0.1,Gamma=0.1
0.25
0.2
0.15
0.1
0.05
0
Power Difference(mW)
3
2.5
2
1.5
1
0.5
0
L(mW)
0
50
100
150
I(mA)
simulated power difference
measured power difference
power without feedback

(b)

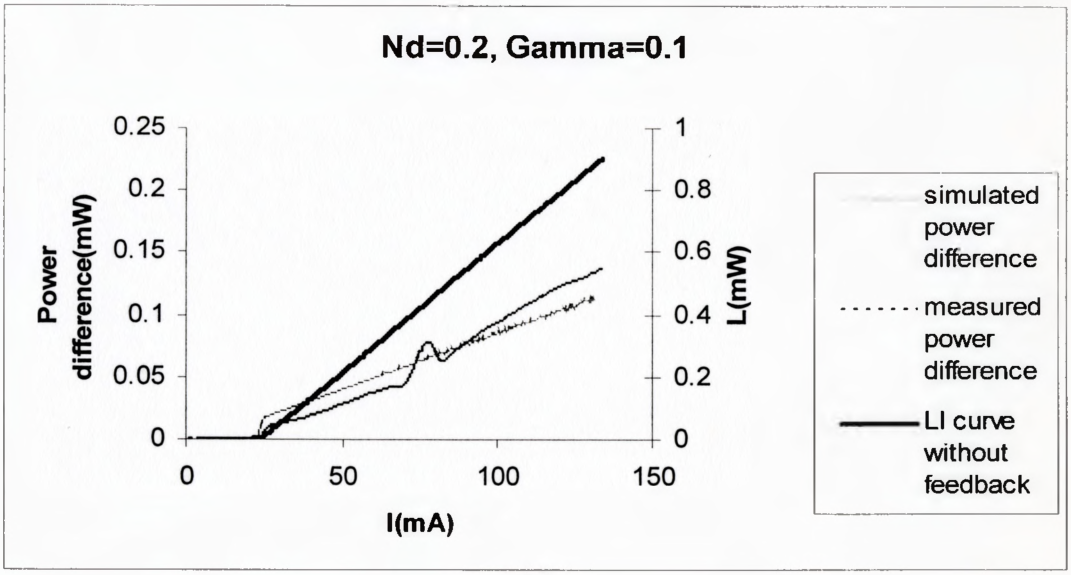
Nd=0.2, Gamma=0.1
0.25
0.2
0.15
0.1
0.05
0
Power difference(mW)
1
0.8
0.6
0.4
0.2
0
L(mW)
0
50
100
150
I(mA)
simulated power difference
measured power difference
LI curve without feedback

(c)

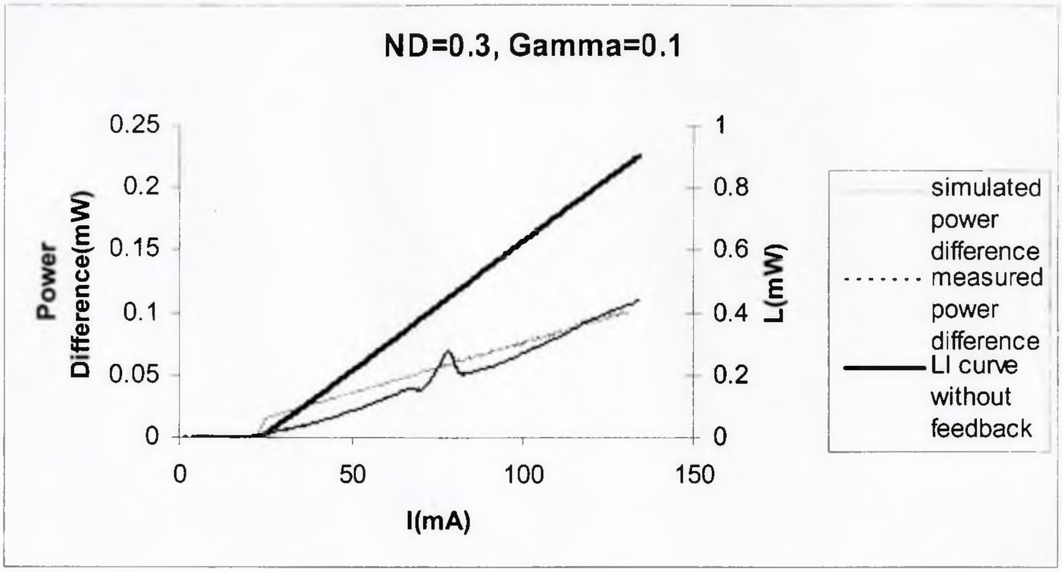

(d)

Fig.4.10 Measurement with ND filter. (a) ND = 0.0, γ = 0.1. (b) ND = 0.1, γ = 0.1. (c) ND = 0.2, γ = 0.1, (d)ND = 0.3, γ = 0.1.

4.4 Discussion

By defining the coherence parameter, we found four factors affecting partial coherent interaction of the feedback light with the field in the laser cavity which is working in "coherence collapse" regime: (1) The length of the external cavity; (2) The bandwidth (FWHM) of the wavelength-dependent-feedback element; (3) The amount of feedback; (4) The injected current.

We applied the FBG with 4% peak reflectivity for the first experiment measurement by fusing the FBG closer or further away from the laser front facet. Through the fitting results, we found that the coherence parameter would get smaller when the length of the external cavity gets larger and *vice versa*.

When changing the feedback element to a mirror, the coherence parameter is much smaller compared with the FBG feedback under the external cavity length. While a blazed grating was applied, the coherence parameter becomes much bigger compared with the FBG feedback for the same distance. We relate this phenomenon to the bandwidth of the feedback elements. The mirror has no wavelength selectivity, therefore it has the widest bandwidth of the three elements. On the other extreme, the blazed grating reflects only one longitudinal mode back to the laser cavity. The bandwidth of the blazed grating in Littrow configuration in our set-up is the narrowest compared with FBG and mirror. The bandwidth of FBG lies in between with FWHM of 1.47 nm. Through these measurements, we can conclude that by changing the bandwidth (FWHM) of the FBG, we can change the part of feedback which is interacting coherently with the field in the laser cavity. The narrower is the bandwidth of the feedback element, the higher the coherence parameter.

We probe the relationship between the amount of feedback and the coherence parameter with a FBG of 73% peak reflectivity under a fixed feedback distance of 200 cm. The amount of feedback was changed by ND filters. We found by measurements and fitting results that when the external cavity length is fixed, the amount of feedback would not change the coherence parameter much and it almost keep constant within the regime of "coherence collapse" from -40 dB~-10 dB. The coherence parameter gets a little bit higher when the amount of feedback increases to an upper limit of ~-10 dB. This is reasonable because when the feedback level increases over -10 dB, the laser will work in regime five in which the linewidth of this configuration is narrowed for all phases of returned light and is generally insensitive to all other reflections.

In summary, when the laser is working in the "coherence collapse" regime, the linewidth is extremely broadened, and thus the coherent length is short (about 10 mm). We conclude by our measurement that the interaction of the feedback light and the field in the laser cavity is still not totally incoherent as people assumed before; the actual mechanism is partial coherent interaction. The coherence parameter was defined as the part of feedback light which is interacting coherently with the field in the laser cavity. We related the coherence parameter to the external cavity length and the bandwidth of the feedback element. Because the coherent length of the laser light would not change much in the "coherence collapse" regime, the coherence parameter decreases as the distance between the feedback mirror and the laser front facet increases. On the other hand, the amount of feedback would not change the coherence parameter much in this region of feedback. The bandwidth of the feedback element embodies its ability of wavelength selectivity. Narrower bandwidth will cause more coherent interaction. The coherence parameter is not constant for all of the injection current, it is a function of the current: $\gamma = \gamma(I)$.

We expect γ to be a function of the length of the pump laser. Longer lasers will have narrower line widths, and hence more coherently interacting light than shorter lasers. This linewidth dependence of γ is similar to the dependence of γ on pumping. Pumping hard tends to reduce the linewidth. Hence long pump lasers, such as high power laser, will have larger γ and may not operate as expected in FBG systems designed for short pump lasers.

CHAPTER 5 CONCLUSION

In this chapter, a summary of work done in this thesis is given, along with recommendation for future work.

5.1 Summary of work

In this thesis, the partially coherent interaction of the feedback light with the field in the laser cavity is affirmed with 980-nm pump lasers. The coherence parameter γ was defined to identify the fraction of feedback light interacting coherently with the field established in the laser cavity. We showed by simulation and measurement that, in contrast to the normally accepted totally incoherent state of operation in the "coherence collapse" regime, there is always a small part of the feedback light working coherently; and different coherence parameters lead to get different slopes in the power difference curve. The value of γ ($0 \leq \gamma \leq 1$) can be determined by fitting the measured power-difference versus pumping-rate curve to the simulation results.

Measurements were done with three feedback elements: fiber Bragg grating, mirror, and blazed grating. Four features of coherence parameter γ were probed: (1) the variation of γ with the length of the external cavity; (2) the variation of γ with the bandwidth (FWHM) of the wavelength-dependent-feedback element; (3) the variation of γ with the amount of feedback; and (4) the variation of γ with the injected current.

Experimental measurements confirmed that the coherence parameter γ decreases while the distance between the FBG and the laser facet increases. γ does not change much with the amount of feedback if the device is kept operating in the "coherence-collapse" regime. The effect of bandwidth of the feedback element was probed by comparing the fitting results of the mirror, the blazed grating and the FBG. By comparing the coherence parameters for the three elements, we found that under the same distance, for the more wavelength-selective feedback like blazed gratings, γ can be much higher than for a mirror whose bandwidth is infinity. FBG has finite bandwidth and then its coherence parameter lies in between that of mirror and blazed grating for the same length of external cavity.

5.2 Recommendation for future work

The characterization of the partial coherent interaction is very important for understanding the long external cavity feedback laser. Based on the work of this thesis, there are many paths which could branch out from it.

This work will be help to improve the performance of the high power FBG stabilized 980-nm pump laser. The relationship between the kink power and the coherence parameter is a promising research direction for the high power FBG stabilized 980-nm pump laser. The incoherent part of feedback cause less mode hoping thus more stable output optical power. The incoherent part is related to the coherence parameter and can be changed by three factors: the peak reflectivity, the bandwidth of the FBG, and the distance between the front facet and the FBG.

The polarization of the feedback light is another concern in this research. Polarization maintaining fiber is recommended to avoid fluctuations in the power difference curve measurement.

References:

[1] G. H. B. Thompson, Chapter 3, "Physics of semiconductor laser devices", JOHN WILEY&SONS, 1980.

[2] C. Lin, C. A. Burrus Jr. and L. A. Coldren, "Charateristics of single-longitudinal mode selection in short-coupled-cavity (SCC) injection lasers", J. Lightwave technol., Vol. LT-2, pp. 544-549, 1984.

[3] S. C. Woodworth, D. T. Cassidy, M. J. Hamp, "Sensitive absorption spectroscopy by use of an asymmetric multiple quantum-well diode laser in an external cavity", Applied Optics, Vol. 40, No. 36, pp. 6719-6724, 2001.

[4] R. S. Vodhanel and J. S. Ko, "Reflection-induced frequency shifts in single-mode laser diodes coupled to optical fibers", Electron. Lett., Vol. 20, pp. 972-974, 1984.

[5] L. Goldberg, H. F. Taylor, A. Dandridge, J. F. Weller, R. O. Wiles, "Spectral characteristics of semiconductor lasers with optical feedbback", IEEE J. Quantum Electronics, Vol. QE-18, No. 4, pp. 555-564, 1982.

[6] L. A. Coldren, G. D. Boyd and C. A. Burrus, "Dependence of chirping on cavity separation in two-section coupled-cavity lasers", Electron. Lett., Vol. 21, pp. 527-528, 1985.

[7] T. Fujita, J. Ohya, K. Matsuda, M. Ishino, H. Sato and H. Serizawa, "Narrow spectral linewidth characteristics of monolithic integrated-passive cavity InGaAsP/InP semiconductor lasers", Electron.Lett., Vol. 21, pp. 374-376, 1985.

[8] K. Petermann, "External optical feedback phenomena in semiconductor lasers", IEEE J. Selected Topics in Quantum Electronics, Vol. 1, No. 2, pp. 480-489, 1995.

[9] K. Peterman, Chapter 9, "Laser diode Modulation and noise".

[10] G. P. Agrawal, "Line narrowing in a single-mode injection laser due to external optical feedback", IEEE J. Quantum Electron., Vol. QE-20, No. 5, pp. 468-476,1984.

[11] P. Spana, S. Piazolla and M. Tamburrini, "Theory of noise in semiconductor lasers in the presence of optical feedback", IEEE J. Quantum Electron., Vol. QE-20, No. 4, pp. 350-357, 1984.

[12] E. Patzak, A. Sygimura, S. Saito, T. Mukai and H. Olesen, "Semiconductor laser linewidth in optical feedback configurations", Electron. Lett., Vol. 19, pp. 1026-1027, 1983.

[13] K. Kikuchi and T. Okoshi, "Simple formula giving spectrum narrowing ratio of semiconductor laser output obtained by optical feedback ", Electron. Lett., Vol. 18, pp. 10-12, 1982.

[14] R. W. Tkach and A. R. Chraplyvy, "Regimes of feedback effect in 1550-nm distributed feedback lasers", J. Lightwave Technol., Vol. LT-4, No. 11, pp. 1655-1661, 1986.

[15] D. Lenstra, B. H. Verbeek, A. J. Denboef, "Coherence collapse in single mode semiconductor lasers due to optical feedback", IEEE J. Quantum. Electron., Vol. QE-21, No. 6, pp. 674-679, 1985.

[16] C. H. Henry, R. T. Kazarinov, "Instability of semiconductor lasers due to optical feedback from distant reflectors", IEEE J. Quantum Electron., Vol. QE-22, No. 2, pp. 294-301, 1986.

[17] A. H. Ngnyen, Ph. D thesis, McMaster University, 1999.

[18] L. J. Bonnell and D. T. Cassidy, "Alignment tolerances of short-external-cavity InGaAsP diode lasers for use as tunable single-mode sources", Appl. Opt., Vol. 28, pp. 4622, 1989.

[19] L. Guo, Master's thesis, McMaster University, 2002.

[20] E. Desurvire, "Spectral noise figure of Er3+-doped fiber amplifiers", IEEE Photon. Technol. Lett., Vol. 2, pp. 208-210, 1990.

[21] B. F. Ventrudo, G. A. Rogers, G. S. lick, P. Hargreaves, T. N. Demayo, "Wavelength and intensity stabilization of 980-nm diode lasers coupled to fiber Bragg gratings", Electron. Lett., Vol. 30, No. 25, pp. 2147-2149, 1994.

[22] M. Achtenhagen, S. Mohrdiek, T. Pliska, N. Matuschek, C. S. Harder, A. Hardy, "L-I characteristics of fiber Bragg grating stabilized 980nm pump lasers", IEEE photonics Technol. Lett., Vol. 13, No. 5, pp. 415-417, 2001.

[23] K. O. Hill, B. Malo, F. Bilodean, D. C. Johnson, "Photosensitivity in optical fibers", Annn, Rev., Mater. Sci, Vol. 23, pp. 125-157, 1993.
[24] T. Erdogan, "Fiber grating spectra", IEEE J. Lightwave Tech., Vol. 15, No. 8, pp. 1277-1294, 1997.
[25] F. N. Timofeev, G. S. Simin, M. S. Shatalov, P. Bayvel, R. Wyatt, I. Lealmeas, R. Kashyap, "Experimental and theoretical study of high temperature-stability and low-chirp 1.55um semiconductor laser with an external fiber grating", Fiber and Intergrated Optics, Vol. 19, pp. 327-353, 2000.
[26] K. O. Hill and G. Meltz, "Fiber Bragg grating technology fundamentals and overview", J. Lightwave Technol., Vol. 15, No. 8, pp. 1263-1276, 1997.
[27] R. O. Miles, A. Dandridge, A. B. Tveten, H. F. Taylor, T. G. Giallorenzi, "Feedback induced line broadening in cw channel substrate planar laser diodes", Appl. Phys. Lett., Vol. 37, pp. 990-992, 1980.
[28] L. Goldberg, H. F. Taylor, A. Dandrige, J. F. Wellwe and R. O. Miles, "Spectral characteristics of semiconductor lasers with optical feedback", IEEE Trans. Microwave Theory Tech., Vol. MTT-30, pp. 401-410, 1980.
[29] D. T. Cassidy, "Influence on the steady state oscillation spectrum of a diode laser for feedback of light interacting coherently and incoherently with the field established in the laser cavity", Appl. Optics, Vol. 23, No. 3, pp. 2070-2077, 1984.
[30] H. Temkin, N. A. Olsson, J. H. Abeles, R. A. logan, M. B. Danish, "Reflection noise in index-guided InGaAsP lasers", IEEE J. Quantum Electron., Vol. QE-22, No. 2, pp. 286-293, 1986.
[31] C. H. Henry, R. F. Kazarinov, "Instability of semiconductor lasers due to optical feedback from distant reflectors", IEEE J. Quantum Eletron., Vol. QE-22, No. 2, pp. 294-301, 1986.
[32] K. O. Hill, Y. Fujii, D. C. Johnson, B. S. Kaunsaki, "Photosensitivity in optical waveguides: Application to reflection fiber fabrication", Appl. Phys. Lett. 32 (10), p 647, 1978.

[33] W. W. Morey, G. Melta and W. H. Glenn, "Holographically generated gratings in optical fibers", Optics & Photonics News, Vol. 1, No. 7, p 8, 1994.

[34] K. O. Hill, B. Malo, F. Bilodeau, D. C. Johnson, J. Albert, "Bragg grating fabricated in monomode photosensitive optical fiber", IEEE J. Quantum Electron., Vol. 62 , No. 10, pp. 1035-1037, Mar 1993.

[35] Y. Qiu, Y. Sheng, C. Beaulien, "Optical phase mask for fiber mask for fiber Bragg gratings fabrication", J. Lightwave Technol., Vol. 17, No. 11, pp. 2366-2370, 1999.

[36] Y. Sheng, J. Wang, Y. Qiu, P. Kung, "Modeling and testing phase mask stitching error for writing fiber gratings", OSA technical Digest on Diffraction Optics and Micro-Optics, pp. 66-68, 2000, Quebec City Canada.

[37] B. J. Eggleton, P. A. Krug, L. Poladian, F. Quellette, "Long period superstructure Bragg grating in optical fibers", Electron. Lett., Vol. 30, pp. 1620-1622, 1994.

[38] F. Ouellette, "Dispersion cancellation using linearly shirped Bragg grating filters in optical waveguides", Opt. Lett, Vol. 12, pp. 847-849, 1987.

[39] T. Erdogan, "Fiber grating spectra", J. Lightwave Technol., Vol. 15, No. 8, pp. 1277-1294, 1997.

[40] D. T. Cassidy, "Comparison of rate equation and Fabry-Perot approaches to modeling a diode laser", Applies Optics, Vol. 22, No. 21, pp. 3321-3326, 1983.

[41] D. T. Cassidy, "Technique of measurement of the gain spectra of semiconductor diode lasers", J. Appl. Phys., Vol. 56 (11), pp. 3096-3099, Dec. 1984.

[42] L. A. Coldren, S. W. Corzine, "diode lasers and photonic intergrated circuits", chapter 3, John Viley and Sons inc., 1995.

[43] B. W. Hakki and T. L. Paoli, "Gain spectra in GaAs double-hetero structure injection lasers", J. Applied Physics, Vol. 46, No. 3, pp. 1299-1306, 1975.

[44] J. E. Hayward, D. T. Cassidy, "Nonlinear gain and the spectral output of short-external-cavity 1.3 um InGaAsP semiconductor diode lasers", IEEE J. Quantum Electron., Vol. 30, No. 9, pp. 2043-2050, 1984.

[45] T. Pliska, N. Matuschek, S. Mohrdiek, A. Hardy, C. Harder, "External feedback optimization by means of polarization control in fiber Bragg grating stabilized 980-nm pump lasers", IEEE Photonics Technol. Lett., Vol. 13, No. 10, pp. 1061-1063, 2001.

[46] D. T. Cassidy, "Front/back tracking in InGaAsP diode laser transmitter modules", J. Lightwave Technol., Vol. 6, No. 9, pp. 1395-1398, 1988.

[47] G. P. Agrawal, "Longitudinal-mode stabilization in semiconductor lasers with wavelength selective feedback", J. Appl. Phys., Vol. 59, pp. 3958-3961, 1986.

[48] R. Ulrich, S. C. Rashleigh, and W. Eickhoff, "Bending-induced birefringence in single-mode fibers", Optics Lett., Vol. 5, No. 6, pp. 273-275, 1980.

[49] G. Genty, A. Grohn, M. Kaivola, H. Ludvigse, "Analysis of the linewidth of a grating-feedback GaAlAs laser", IEEE J. Quantum. Electron. , Vol. 36, No. 10, pp. 1193-1198, 2000.

[50] A. S. van de Nes, J. J. H. B. Schleipen, G. W.'t Hooft, M. P. van Exter, "Feedback effects at stable and unstable resonant external cavity lengths", IEEE J. Quantum Electron., Vol. 38, No. 8, pp. 1097-1101, 2002.

[51] J. E. Hayward, D. T. Cassidy, "Experimental confirmation of internal scattering as a dominant mechanism determining the longitudinal mode spectra of 1.3μm semiconductor diode lasers", J. Opt. Soc. Am. B., Vol. 9, No. 7, pp. 1151-1157, 1992.

[52] F. H. Peters and D. T. Cassidy, "Scattering, absorption, and anomalous spectral tuning of 1.3μm semiconductor diode lasers", J. Appl. Phys., Vol. 71, No. 9, pp. 4140-4144, 1992.

[53] G. B. Morrison, D. T. Cassidy, "A probability-amplitude transfer matrix model for distributed-feedback laser structures", IEEE J. Quantum Electron., Vol. 36, No. 6, pp. 633-640, 2000.